Electronic structure and heat transport of multivortex configurations in mesoscopic superconductors

A. S. Mel'nikov, D. A. Ryzhov, and M. A. Silaev
Institute for Physics of Microstructures, Russian Academy of Sciences, 603950 Nizhny Novgorod GSP-105, Russia
(Received 4 April 2008; revised manuscript received 27 June 2008; published 13 August 2008)

On the basis of the Bogoliubov–de Gennes theory we study the transformation of the quasiparticle spectrum in the mixed state of a mesoscopic superconductor, governed by an external magnetic field. We analyze the low-energy part of the excitation spectrum and investigate the field dependent behavior of anomalous spectral branches crossing the Fermi level. Generalizing the Caroli–de Gennes–Matricon approach, we present an analytical solution describing the anomalous branches in a vortex with an arbitrary winding number. We also study the spectrum transformation caused by the splitting of a multiquantum vortex into a set of well separated vortices focusing mainly on a generic example of a two-vortex system. For vortices positioned rather close to the sample surface we investigate the effect of the quasiparticle reflection at the boundary on the spectrum and the density of states at the Fermi level. Considering an arbitrary surface curvature, we study the disappearance of an anomalous spectral branch for a vortex leaving the sample. The changes in the vortex configuration and resulting transformation of the anomalous branches are shown to affect strongly the density of states and the heat conductance along the magnetic-field direction.

DOI: 10.1103/PhysRevB.78.064513 PACS number(s): 74.25.Op, 74.78.Na, 74.25.Fy

I. INTRODUCTION

Modern technology development provides a unique possibility to study exotic vortex states in mesoscopic superconducting samples of the size of several coherence lengths.[1–3] Tuning the external applied magnetic field one can switch between rich varieties of energetically favorable or metastable vortex configurations, which cannot be realized in bulk systems. Of particular interest is a possibility to obtain multiquanta (giant) vortex states with winding numbers larger than unity for certain intervals of external magnetic field (see, e.g., Ref. 2). The merging of individual vortices into a multiquantum one occurs under the influence of screening currents, which push the vortices to the sample center. Note that alternatively the stable multiquanta vortices can appear even in a bulk superconductor because of the pinning on columnar defects with radii of the order of the coherence length.[4] Experimentally the vortex configurations in mesoscopic systems and the phase transitions between them can be studied, e.g., by Hall-probe measurements of the branching of the magnetization curve[3] or by observation of the vortex entry into the sample using the point-contact techniques.[5]

Changing the number and arrangement of the flux lines we can tune the low-energy excitation spectrum, which is known to be responsible for low-temperature thermodynamic and transport properties of the sample. The mechanism of such changes in the subgap quasiparticle spectrum is associated with the modification of the anomalous energy branches crossing the Fermi level. For well separated vortices positioned at distances much larger than the core radius, the behavior of the anomalous branches can be described by the Caroli–de Gennes–Matricon (CdGM) theory.[6] For each individual vortex the energy $\varepsilon(\mu)$ of a subgap state varies from $-\Delta_0$ to $+\Delta_0$ as one changes the angular momentum μ defined with respect to the vortex axis. At small energies $|\varepsilon| \ll \Delta_0$ the spectrum is a linear function of μ: $\varepsilon(\mu) \simeq -\mu\omega$, where $\omega \approx \Delta_0/(k_\perp \xi)$ [Δ_0 is the superconducting gap value far from the vortex axis, $k_\perp = \sqrt{k_F^2 - k_z^2}$ (k_F is the Fermi momentum and k_z is the momentum projection on the vortex axis) $\xi = \hbar V_F/\Delta_0$ is the coherence length (V_F is the Fermi velocity)] and μ is half an odd integer.

With the decrease in the intervortex distance the quasiparticle tunneling between the vortex cores comes into play resulting in the modification of the anomalous branches.[7] Finally, when the vortex cores merge one obtains a multiquantum vortex with a certain winding number M. The number of anomalous branches per spin projection[8] is conserved during this process of crossover from M individual flux lines to the M-quantized giant vortex and equals the vorticity M. Previously, the behavior of the anomalous branches in a multiquantum vortex has been investigated numerically[9] and analytically for a steplike model profile of the order parameter in the core.[10] For vortices with an even vorticity all the anomalous branches cross the Fermi level at nonzero impact parameters $b = -\mu/k_\perp$;

$$\varepsilon(\mu) \sim -(\mu \pm \mu_j)\Delta_0/(k_\perp \xi), \tag{1}$$

where $j = 1 \ldots M/2$ and $\mu_{M/2} \sim k_\perp \xi$. For a vortex with an odd winding number there appears a branch crossing the Fermi level at zero impact parameter.

The wave functions of the subgap states are localized inside the vortex core because of the Andreev reflection of quasiparticles at the core boundary. Any additional normal scattering process should modify the behavior of the anomalous spectral branch. Such modification can be caused even by atomic size impurities, as it was predicted by Larkin and Ovchinnikov in Ref. 11. For a vortex approaching a flat sample boundary the distortion of the local density-of-states (DOS) profile has been analyzed in Ref. 12 numerically on the basis of the Eilenberger theory both for s-wave and d-wave pairing symmetries. Certainly the role of normal scattering at the boundaries can be of particular importance

for vortices trapped in mesoscopic samples. For a single vortex placed in a superconducting cylinder an appropriate spectrum transformation was studied in Refs. 13 and 14.

Experimentally the behavior of the anomalous branches can be probed, e.g., by the scanning tunneling microscopy (STM) or by the heat transport measurements. The modern STM technique is a unique tool for the study of the local DOS profiles and, thus, could provide us the information about the number and configuration of the spectral branches crossing the Fermi level. An important advantage of the heat conductance measurements along the vortex lines is associated with the fact that probing the number and transparency of quasiparticle transport channels this method appears to be sensitive also to the k_z dispersion of the spectrum and, in particular, to the group velocity of quasiparticle modes propagating along the vortex cores.[14,15] Indeed, it is the small group velocity of CdGM states that is responsible for a strong suppression of the heat conductance $\kappa_v \sim T^2 k_F \xi/(\hbar \Delta_0)$ along a singly quantized vortex core as compared to the Sharvin conductance $\kappa_{\mathrm{Sh}} \sim T(k_F \xi)^2/\hbar$ of a normal-metal wire of the radius ξ at certain temperature T:

$$\frac{\kappa_v}{\kappa_{\mathrm{Sh}}} \sim \frac{1}{k_F \xi} \frac{T}{\Delta_0} \ll 1. \tag{2}$$

Within the Landauer approach such suppression of the vortex heat conductance can be understood as a consequence of a strong reduction in the effective number of conducting modes $N_v = \kappa_v/\kappa_0$, where $\kappa_0 = \pi T/(3\hbar)$ is the universal heat conductance per conducting mode in a normal metal. Taking the interlevel spacing $\omega_0 \approx \Delta_0/(k_F \xi)$ for the anomalous branch at $k_z = 0$, one obtains $N_v \sim T/\omega_0$—which agrees with the above estimation [Eq. (2)]. Both the intervortex quasiparticle tunneling and the normal scattering at the sample boundary are expected to affect the effective number of conducting modes resulting in the dependence of the heat transport on the vortex configuration in a mesoscopic superconductor. The increase in the heat conductance stimulated by the boundary effects was demonstrated in Ref. 14 for a single vortex state in a cylinder.

It is the goal of the present paper to study both the transformation of the anomalous branches and distinctive features of the DOS and heat transport in different multivortex configurations in mesoscopic samples. We include in our consideration both the spectrum transformation caused by the giant vortex splitting and the process of an anomalous branch formation (disappearance), which occurs when a vortex enters (exits) the sample. In the present study we address only the case of homogeneous mesoscopic superconductors without any defects or pinning centers.

The paper is organized as follows: To elucidate our main results we start from a qualitative discussion of the behavior of the anomalous branches in a mesoscopic superconductor (see Sec. II). In Sec. III we introduce the basic equations used for the spectrum calculation. In Sec. IV we consider an analytical solution describing the spectrum of a multiquantum vortex line. In Sec. V we study a generic example of the spectrum transformation caused by the decay of giant vortices, i.e., the splitting of a doubly quantized vortex into two individual singly quantized vortices. The influence of the normal reflection at the sample surface on the quasiparticle spectrum for a vortex positioned close to the boundary is analyzed in Sec. VI. In Secs. VII and VIII we calculate the density of states and the thermal conductance, respectively, using the quasiparticle spectra found in the previous sections. We summarize our results in Sec. IX. Some of the details of our calculations are given in appendices.

II. TRANSFORMATION OF ANOMALOUS SPECTRAL BRANCHES: QUALITATIVE PHYSICAL PICTURE

As we discussed in Sec. I there are two basic mechanisms responsible for the transformation of anomalous branches in a multivortex configuration: (i) the tunneling of quasiparticles between the vortex cores and (ii) the quasiparticle scattering at the sample boundaries, which comes into play when the vortices approach the superconductor surface. To clarify the key physical consequences of these mechanisms hereafter, we consider two model problems: (i) electronic structure of a multivortex system positioned rather far from the boundary and (ii) electronic structure of an individual vortex approaching the sample surface.

A. Effect of intervortex quasiparticle tunneling

Let us start with a qualitative analysis of the behavior of the anomalous branches and consider a set of vortex lines parallel to the z axis. It is the case of intermediate values of magnetic field when vortices are quite far from the boundary but do not merge into a multiquantum vortex. In the (xy) plane the vortex centers defined as points of the order-parameter phase singularities (and hence as zeros of the superconducting order parameter) are positioned at certain coordinates $\mathbf{r}_i$.

The system is homogeneous in the z direction and, as a result, the momentum k_z appears to be conserved. The two-dimensional quantum-mechanical problem in the (xy) plane can be strongly simplified provided the wavelength $k_\perp^{-1}$ is much less than the superconducting coherence length ξ. Thus, following standard quasiclassical procedure (see Sec. III for details) one can describe the quantum mechanics of quasiparticles using the geometrical optics picture. An important distinctive feature of this picture in superconductors is that all the classical trajectories can be approximately considered as straight lines. The bending of these straight trajectories is negligible because of a small momentum change $\delta k \sim 1/\xi$ during the process of quasiparticle scattering at the inhomogeneous superconducting gap profile, i.e., during the Andreev reflection. We also can neglect the trajectory bending caused by magnetic field, since we assume the cyclotron radius $r_H \sim V_F/\omega_H \sim k_F \xi^2 (H_{c2}/H)$ to exceed all the relevant length scales of our problem. Here $\omega_H = |e|H/(mc)$ is the cyclotron frequency, m is the electron effective mass, and H_{c2} is the upper critical field.

For quasiparticles propagating along the classical trajectories parallel to $\mathbf{k}_\perp = k_\perp(\cos\theta_p, \sin\theta_p)$, we introduce the angular momenta $\mu = [\mathbf{r}, \mathbf{k}_\perp]\cdot \mathbf{z_0} = k_\perp r \sin(\theta_p - \theta)$ and $\tilde{\mu}_i = \mu - [\mathbf{r}_i, \mathbf{k}_\perp]\cdot \mathbf{z}_0$ defined with respect to the z axis passing through the origin and with respect to the ith vortex axis

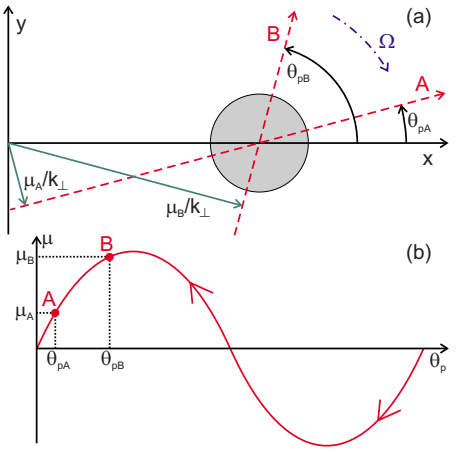

FIG. 1. (Color online) Schematic plot of trajectory precession around vortex line (a) in real space and corresponding quasiclassical orbit for $\varepsilon=0$ (b) in the (μ,θ_p) plane. Vortex core is shown by gray circle.

passing through the point $\mathbf{r}_i$, correspondingly $[(r,\theta,z)$ is the cylindrical coordinate system]. Neglecting the quasiparticle tunneling between the vortex cores and the normal scattering at the sample boundary, we get degenerate CdGM energy branches: $\varepsilon_i=-\omega\tilde{\mu}_i$ for $|\varepsilon|\ll\Delta_0$. For a fixed energy ε we can define a set of crossing quasiclassical orbits in the plane (μ,θ_p): $\mu_i(\theta_p)=-\varepsilon/\omega+[\mathbf{r}_i,\mathbf{k}_\perp]\cdot\mathbf{z}_0$.

The quasiclassical orbit in the (μ,θ_p) plane for a single Abrikosov vortex is shown in Fig. 1(b). Each point at this orbit corresponds to a straight trajectory passing through the vortex core [Fig. 1(a)]. Precession of the quasiclassical trajectory is described by the Hamilton equation: $\hbar\partial\theta_p/\partial t=\partial\varepsilon/\partial\mu$, which provides us the precession frequency $\Omega=-\omega/\hbar$. This precession is a result of the small deviation from the exact Andreev backscattering of quasiparticles in the vortex core. In Fig. 1(b) the direction of the trajectory precession is shown by arrows. The discrete spectrum of subgap quasiparticle states can be found using the Bohr-Sommerfeld rule. In the case of several vortices we have several crossing quasiclassical orbits in the (μ,θ_p) plane. These orbits are shown by dash lines in Fig. 2(a) for a particular case of two vortices with $\mathbf{r}_1=(-a/2,0)$ and $\mathbf{r}_2=(a/2,0)$. Each crossing point of quasiclassical orbits $\mu_i(\theta_p)$ and $\mu_j(\theta_p)$ correspond to the trajectories passing through the cores of ith and jth vortices. It is natural to expect that the

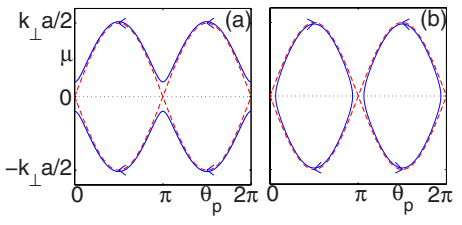

FIG. 2. (Color online) Schematic plots of quasiclassical orbits for $\varepsilon=0$ in the (μ,θ_p) plane (solid lines) for (a) two vortices with intervortex distance a and (b) vortex near the flat surface ($a/2$ is the distance between vortex and surface). The orbits for two noninteracting vortices are shown by dashed lines.

degeneracy at these points will be removed if we take account of a finite probability of quasiparticle tunneling between the cores. Let us consider the vicinity of the degeneracy point, e.g., $\theta_p=0$ [see Fig. 2(a)]. The trajectory characterized by the angle $|\theta_p|\ll\xi/a$ passes through both vortex cores, and therefore the wave function along such trajectories can be found as a superposition of two states localized at different vortices and having close energies: $\varepsilon_{v1}=-\omega[\mu-(k_\perp a/2)\sin\theta_p]$ and $\varepsilon_{v2}=-\omega[\mu+(k_\perp a/2)\sin\theta_p]$. The transformation of the quasiclassical spectrum occurring due to the overlapping of the corresponding wave functions can be described using a standard quantum-mechanical approach describing a two-level system—[16] which yields the secular equation,

$$(\varepsilon-\varepsilon_{v1})(\varepsilon-\varepsilon_{v2})=(\delta\varepsilon)^2, \tag{3}$$

and results to the splitting of isoenergetic lines near the degeneracy point ($\theta_p=0$ for our example):

$$\varepsilon=-\omega\mu\pm\sqrt{\omega^2(k_\perp a/2)^2\theta_p^2+(\delta\varepsilon)^2}. \tag{4}$$

The tunneling of quasiparticles between vortex cores is determined by the exponentially small overlapping of wave functions localized near the cores and results in the splitting of energy levels: $\delta\varepsilon\sim\Delta_0\exp[-k_F a_{ij}/(k_\perp\xi)]$, where $a_{ij}=|\mathbf{r}_i-\mathbf{r}_j|$ is the distance between vortex lines and $k_F a_{ij}/k_\perp$ is the distance between vortex centers along the trajectory. The estimate for the splitting $\delta\mu\simeq\delta\varepsilon/\omega$ of isoenergetic lines in the (μ,θ_p) plane reads [see Eq. (4)]:

$$\delta\mu(a_{ij})\sim k_\perp\xi\exp\left(-\frac{k_F a_{ij}}{k_\perp\xi}\right). \tag{5}$$

As a result, we get the orbits $\mu_i^*(\theta_p)$ with a qualitatively new behavior [solid lines in Fig. 2(a)]: each of these orbits consists of parts corresponding to the classical quasiparticle trajectories passing through the cores of different vortices.

The tunneling between the cores of the different vortices becomes significant when the energy splitting $\delta\varepsilon$ is comparable to the interlevel spacing ω_0, i.e., when $\delta\mu\gtrsim 1$ in Eq. (5). According to the above condition on $\delta\mu(a_{ij})$ the tunneling is most efficient for $k_\perp=k_F$ and $a_{ij}<a_c$, where $a_c\simeq\xi\ln(k_F\xi)$ is a critical intervortex distance. Using the percolation theory language, we can consider the vortices to be bonded if $a_{ij}<a_c$, and we can define a cluster in a flux line system as a set of M vortices bonded either directly or via other vortices. Certainly in mesoscopic superconductors the cluster dimensions L_v cannot exceed the sample size. The cluster is characterized by a set of hybridized quasiparticle states: with a change in the $\mathbf{k}_\perp$ direction the wave function experiences a number of subsequent transitions between the cores of neighboring vortices. Taking, e.g., the upper quasiclassical orbit in Fig. 2(a), we obtain the wave function concentrated near the cores of the right and left vortices for the angular intervals $0<\theta_p<\pi$ and $\pi<\theta_p<2\pi$, respectively. Further decrease in the intervortex distance results in the increase in the tunneling probability and, thus, the increase in $\delta\mu(a_{ij})$. Finally, for $a_{ij}\to 0$ we get a set of M lines $\mu=$const parallel to the θ_p axis, i.e., M anomalous branches crossing zero energy at angular independent impact param-

eters and corresponding to the M-quantum vortex. Certainly this limit can be realized only in mesoscopic samples.

Within the quasiclassical approach one can estimate the intervortex tunneling efficiency using the Landau-Zener transition theory. Let us consider the vicinity of the degeneracy point, e.g., $\theta_p=0$ [see Fig. 2(a)]. The tunneling probability of transition from one quasiclassical orbit to another is given by the expression,[16]

$$W = \exp\left[-4\ \mathrm{Im}\int_0^{i\theta_p^*} \mu(\theta_p) d\theta_p \right], \tag{6}$$

where $\theta_p^*=2\delta\varepsilon/(\omega k_\perp a)$ and $\mu(\theta_p)$ should be taken from Eq. (4) with lower sign. Finally, we obtain the following estimate for the tunneling probability:

$$W = \exp[-2\pi(\delta\mu/\Delta\mu)^2], \tag{7}$$

where $\Delta\mu=\sqrt{k_\perp a}$ is the quantum-mechanical uncertainty of the angular momentum. Therefore, we can neglect the tunneling between quasiclassical orbits while $\delta\mu \gtrsim \Delta\mu$.

Following Ref. 17 one can obtain the discrete energy levels by applying the Bohr-Sommerfeld quantization rule for canonically conjugate variables μ and θ_p:

$$\int_0^{2\pi n_\theta} \mu(\theta_p) d\theta_p = 2\pi(n+\beta), \tag{8}$$

where n and n_θ are integers, $2\pi n_\theta$ is the period of the $\mu(\theta_p)$ function ($1 \le n_\theta \le M$), and β is of the order unity. The period of $\mu(\theta_p)$ can be larger than $2\pi(n_\theta>1)$ if the Landau-Zener transitions between quasiclassical orbits are not negligible. Depending on the ratio $\delta\mu/\Delta\mu$ one should apply this quantization rule either to the orbits $\mu_i(\theta_p)$ or to the orbits $\mu_i^*(\theta_p)$. In the momentum region,

$$k_F\sqrt{1-[\min(a_{ij})/a_c]^2} \ll |k_z| < k_F, \tag{9}$$

we can neglect the splitting of isoenergetic lines [$\delta\mu \ll \Delta\mu$]. For this region, Equation (8) written for the orbits $\mu_i(\theta_p)$ gives us the CdGM spectrum with a minigap $\omega_0/2=\omega(k_z=0)/2$. For $\min(a_{ij})>a_c$ the CdGM expression holds for the entire momentum range. For vortices forming a cluster the quasiparticle states bonded by intervortex tunneling appear in a finite momentum interval $|k_z|<k_z^*$, where

$$k_z^* = k_F\sqrt{1-[\min(a_{ij})/a_c]^2}. \tag{10}$$

In this limit the quasiparticle tunneling between the cores results in the qualitative modification of spectrum, which can be obtained by substituting $\mu_i^*(\theta_p)$ into Eq. (8):

$$\varepsilon_{ni}(k_z) \approx \frac{\Delta_0}{\xi}\left[\frac{n+\beta}{k_\perp} + b_i(\mathbf{r}_1, \ldots \mathbf{r}_M)\right], \tag{11}$$

where $i=1 \ldots M$. The spectrum Eq. (11) is similar to the one of a multiquanta vortex,[8–10] which recovers in the limit $a_{ij} \to 0$ when $|b_i| \lesssim \xi$. The multivortex cluster geometry and its size L_v determine the effective impact parameters $b_i(\mathbf{r}_1, \ldots \mathbf{r}_M)$, which vary in the range $-L_v \lesssim b_i \lesssim L_v$. Taking a two-vortex (three-vortex) cluster with $\xi<a<a_c$ as an example, we get $b_{1,2} \sim \pm a$ ($b_{1,3} \sim \pm a$, $b_2=0$). Contrary to the CdGM case the spectrum branches [Eq. (11)] can cross the Fermi level as functions of k_z as we decrease the intervortex distance a and minigap is suppressed. The DOS consists of M sets of van Hove singularities corresponding to the extrema of $\varepsilon_{ni}(k_z)$ branches. The energy interval between the peaks belonging to each set is ω_0. For a fixed energy the DOS as a function of a exhibits oscillations with the period of the order of the atomic length scale. Experimentally the intervortex distance can be controlled by a varying magnetic field. For typical values $a \sim \sqrt{\phi_0/H}$ we get the following field scale of DOS oscillations: $\delta H/H \sim \sqrt{\hbar\omega_H/\varepsilon_F}$, where ε_F is the Fermi energy. The oscillatory behavior should affect both thermodynamic and transport properties at low temperatures although, in real experimental conditions, the DOS peak structure is certainly smeared due to the various mechanisms of level broadening, e.g., finite temperature, fluctuations in vortex positions, impurity scattering effects, etc. It should be noted that for typical values $k_F\xi=10^2-10^3$ the critical distance $a_c/\xi \sim 4-6$ exceeds the core radius and the spectrum transformation starts at the fields $H \sim \phi_0/a_c^2 \sim H_{c2}[\ln(k_F\xi)]^{-2}$ when the vortices are indeed well separated.

B. Effect of normal reflection of quasiparticles at the boundary

The above discussion of the behavior of anomalous branches assumed a negligible role of the normal scattering of quasiparticles at the sample boundary. Such assumption is certainly not valid when the intervortex distance becomes so large that some of the individual vortices approach the sample boundary and their spectrum is determined by the interplay of Andreev reflection and normal scattering at the boundary. For rather small samples this interplay can influence the spectrum even for a vortex positioned at the sample center.[13,14]

In order to focus on the role of the boundary effects we consider a model situation when the intervortex quasiparticle tunneling can be neglected (i.e., $a_{ij}>a_c$) because of the rather large cluster size. Thus, we can study the spectrum modification for a single vortex approaching the boundary characterized by a certain curvature in the plane perpendicular to the vortex axis (see Fig. 3). For the sake of simplicity we restrict ourselves to the case of a smooth and specularly reflecting surface. Obviously the quasiclassical spectrum should be disturbed most strongly for trajectories, which return back to the vortex core after the normal reflection at the boundary. These trajectories experience the reflection from a rather narrow surface region near the point positioned at the surface at a minimal distance d from the vortex center. In this region we may consider the surface profile as a parabolic cylinder with a certain focal distance F. Introducing a polar coordinate system (r,θ) with the origin in the vortex center, one obtains the following equation describing this parabolic cylinder at small θ angles: $r(\theta)=d\{1+[1/2+d/(4F)]\theta^2\}$. Note that we should put $d/F>-2$ so that the distance d is indeed the minimal distance to the surface. As it is shown in Fig. 3 the vortex center is positioned at the optical axis of the parabolic mirror. The trajectories experiencing normal reflection and passing twice through the core can be considered within the paraxial approximation.

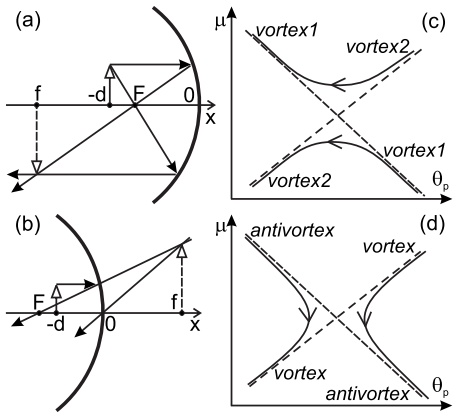

FIG. 3. The geometrical optics analogy for the reflection of quasiclassical trajectories at the concave ($F<0$) parabolic boundary (left panel) and the corresponding modification of the isoenergetic lines (right panel) for $d>-F$ (a) and (c); and for $d<-F$ (b) and (d).

In this case the scattering rules for trajectories reflecting from the surface can be obtained by employing an analogy with a textbook picture describing the system of rays and images in geometrical optics. For a particular case of a concave parabolic mirror ($F<0$) the system of rays is schematically shown in Figs. 3(a) and 3(b). For the object (white solid arrow) situated at the distance d from the mirror the image (white dashed arrow) is formed by the reflected rays at the coordinate $f=-d/h$, where $h=-(1+d/F)$. The type of image is determined by the sign of h: if $h>0$ the image is real, i.e., it has the coordinate $f<0$ and is situated at the same side of the mirror relative to the object [see Fig. 3(a)], otherwise the image is virtual with $f>0$ and situated at the other side of the mirror [see Fig. 3(b)]. Using these well-known results the parameters of reflected trajectories can be derived from the simple trigonometry.

Let us consider the trajectory that makes a small angle $|\theta_p|\ll 1$ with the x axis and has a small impact parameter $|b|\ll d$. Then, the reflected trajectory has the angle $\tilde{\theta}_p=\pi+h\theta_p$ and its impact parameter is $\tilde{b}=hb$. The impact parameters of incident and reflected trajectories are defined relative to the point $\theta=0$ and $r=d$ positioned at the surface at the minimum distance to the vortex center. This point coincides with the coordinate system origin in Figs. 3(a) and 3(b).

In the (μ,θ_p) plane one can define isoenergetic lines corresponding to the incident and reflected trajectories. The intersection of these lines occurring for $|\theta_p|\ll 1$ corresponds to the situation when both the incident and reflected trajectories pass through the vortex core. The degeneracy at the intersection point should be removed by the splitting of isoenergetic lines due to the interaction of vortex core states. One can obtain two qualitatively different regimes of splitting, determined by the ratio between the focal distance F of the parabolic mirror and the distance from the vortex to the surface d, i.e., by the sign of h. The splitting corresponds to the continuous transition from one isoenergetic line to another. The velocity of motion along isoenergetic lines is determined by the angular velocities of trajectory precession, given by $\Omega=\partial\theta_p/\partial t$ and $\tilde{\Omega}=\partial\tilde{\theta}_p/\partial t=h\Omega$ for the incident and reflected trajectories, correspondingly. Therefore, if Ω and $\tilde{\Omega}$ have the same signs ($h>0$), then the directions of precession of the incident and reflected trajectories coincide. In this case, the orbit transformation is analogous to the one that have been obtained for the pair of interacting vortices [Figs. 2(a) and 3(c)]. Otherwise, if $h<0$, the incident and reflected trajectories precess in different directions, therefore the splitting occurs as shown in Figs. 2(b) and 3(d) analogously to the transformation of isoenergetic lines, which can be obtained for the interacting vortex and antivortex.

To study the spectrum transformation, let us consider in detail the simplest configuration: the vortex line is situated at the point $(-a/2,0)$ near the flat boundary of superconductor, occupying the half space $x<0$. If we neglect the normal reflection of quasiparticles at the boundary, the isoenergetic line in the (μ,θ_p) space is given by $\mu_v(\theta_p)=-\varepsilon/\omega-(k_\perp a/2)\sin\theta_p$ [shown for the particular case $\varepsilon=0$ by the dash line in Fig. 2(b)]. The flat boundary is characterized by the infinite focal distance: $F=\infty$; therefore $h=-1$. We obtain the mapping of incident and reflected trajectories according to the following rule: $\tilde{b}=-b$ and $\tilde{\theta}_p=\pi-\theta_p$. Then, we obtain another isoenergetic line: $\mu_{\mathrm{av}}(\theta_p)=-\mu_v(\pi-\theta_p)=\varepsilon/\omega+(k_\perp a/2)\sin\theta_p$, which corresponds to the reflected trajectories and is shown in Fig. 2(b) by another dashed curve. Note that the isoenergetic line $\mu_{\mathrm{av}}(\theta_p)$ (with the opposite direction of trajectory precession) coincides with the isoenergetic line corresponding to an antivortex placed at the point $(0,a/2)$ outside the superconductor. It means that the spectrum of the vortex near the flat surface can be obtained considering the spectrum of the vortex-antivortex system. Indeed, the pair potential of the vortex-antivortex system is invariant under the reflection at the $x=0$ plane: $\Delta(x,y)=\Delta(-x,y)$, yielding the symmetry of the quasiparticle wave function: $\hat{\Psi}(x,y)=\pm\hat{\Psi}(-x,y)$. The odd wave functions obey the boundary condition $\hat{\Psi}(0,y)=0$ while the even wave functions obey the boundary conditions $\partial\hat{\Psi}(0,y)/\partial x=0$. The energy levels corresponding to the even wave functions should be omitted in order to obtain the spectrum of the vortex near the surface. The isoenergetic lines $\mu_{v,\mathrm{av}}(\theta_p)=\pm[\varepsilon/\omega+(k_\perp a/2)\sin\theta_p]$ intersect at certain points, e.g., at $\theta_p=\pi n$ for $\varepsilon=0$, where n is the integer. The degeneracy at these points is removed by the splitting of isoenergetic lines, shown in Fig. 2(b) by the solid lines. Considering the interaction of the two quantum states with close energies $\varepsilon_v=-\omega[\mu+(k_\perp a/2)\sin\theta_p]$ and $\varepsilon_{\mathrm{av}}=\omega[\mu-(k_\perp a/2)\sin\theta_p]$, we obtain again the secular Eq. (3) with $\varepsilon_{v1}=\varepsilon_v$ and $\varepsilon_{v2}=\varepsilon_{\mathrm{av}}$. Therefore, the quasiclassical orbits near the degeneracy point $\theta_p=0$ are given in this case by the following expression:

$$\varepsilon=\pm\sqrt{(\omega\mu)^2+(\delta\varepsilon)^2}-\omega(k_\perp a/2)\theta_p. \tag{12}$$

The classically forbidden angular domain at $\varepsilon=0$ has the width $\delta\theta_p=4\delta\varepsilon/(\omega k_\perp a)$. One can assume that the appearance of such classically forbidden domain explains the deep structure in the local DOS profile observed numerically in Ref. 12 for a vortex near the flat boundary of an s-wave superconductor. As we show below, the classically forbidden angular domain results in the suppression of the overall DOS and we propose that this mechanism should be responsible

for the anomalous spectrum branch disappearance when the vortex exits the sample.

To estimate the tunneling probability between the quasiclassical orbits, we again apply the theory of Landau-Zener transitions. The Landau-Zener tunneling probability is expressed as follows:

$$W = \exp\left[-4\ \mathrm{Im} \int_0^{i\mu^*} \theta_p(\mu) d\mu \right], \tag{13}$$

where $\mu^* = \delta\varepsilon/\omega$ and $\theta_p(\mu)$ should be taken from Eq. (12) with the upper sign. Finally, we obtain the tunneling probability as $W \sim \exp[-2\pi(\delta\theta_p/\Delta\theta_p)^2]$, where $\Delta\theta_p \sim (k_\perp a)^{-1/2}$ is the quantum-mechanical uncertainty of the trajectory orientation angle. Thus, we can neglect Landau-Zener effects while $\delta\theta_p \gtrsim \Delta\theta_p$—i.e., for $a < a_c$, where $a_c \sim \xi \ln(k_\perp \xi)$ is the critical distance, appears to be the same as for a two-vortex system.

III. ANDREEV EQUATIONS

Our further consideration is based on the Bogoliubov–de Gennes (BdG) equations for particle (u) and hole-like (v) parts of the wave function, which have the following form:

$$-\frac{\hbar^2}{2m}(\nabla^2 + k_F^2)u + \Delta(\mathbf{r})v = \varepsilon u,$$

$$\frac{\hbar^2}{2m}(\nabla^2 + k_F^2)v + \Delta^*(\mathbf{r})u = \varepsilon v. \tag{14}$$

Here $\Delta(\mathbf{r})$ is the gap function and $\mathbf{r}=(x,y)$ is a radius vector in the plane perpendicular to the magnetic-field direction. We assume the system to be homogeneous along the z axis, thus, the k_z projection of the momentum is conserved and the wave function takes the form:

$$(u,v) = e^{ik_z z}\hat{\Psi}(\mathbf{r}).$$

Then, the two-component wave function $\hat{\Psi}$ in the momentum representation can be written as follows:

$$\hat{\Psi}(\mathbf{r}) = \frac{1}{(2\pi\hbar)^2} \int \int_{-\infty}^{\infty} e^{i\mathbf{p}\mathbf{r}/\hbar} \hat{\psi}_{\mathbf{p}} d^2\mathbf{p}. \tag{15}$$

Let us introduce the polar coordinate system in momentum space $\mathbf{p}=p(\cos\theta_p, \sin\theta_p)=p\mathbf{p}_0$. Then, the coordinate operator can be written as follows:

$$\hat{\mathbf{r}} = i\hbar\frac{\partial}{\partial\mathbf{p}} = i\hbar\left(\mathbf{p}_0\frac{\partial}{\partial p} + \frac{i}{p}[\mathbf{z}_0,\mathbf{p}_0]\hat{\mu} \right),$$

where operator $\hat{\mu}$ of z projection of angular momentum is given by the expression:

$$\hat{\mu} = \frac{1}{\hbar}[\mathbf{r},\mathbf{p}]\mathbf{z}_0 = -i\frac{\partial}{\partial\theta_p}. \tag{16}$$

Next, we assume that the quasiparticle wave function can be viewed as a wave packet with momenta absolute values close to $\hbar k_\perp$. This assumption is valid with very good accuracy in most superconductors since the characteristic length scale of envelopes of quasiparticle waves is determined by the superconducting coherence length ξ, which is typically much larger than the quasiparticle wavelength ($k_F\xi \gg 1$). Therefore, one can put $p=\hbar k_\perp + q$ ($|q| \ll \hbar k_\perp$) and obtain:

$$\hat{\mathbf{r}} = i\hbar\mathbf{p}_0\frac{\partial}{\partial q} + \frac{i}{2k_\perp}\left\{ [\mathbf{z}_0,\mathbf{p}_0], \frac{\partial}{\partial\theta_p} \right\},$$

where $\{\ldots\}$ is an anticommutator. Of course, such approximation is broken for a very small portion of quasiparticles, which propagate very close to the vortex axis [$2\pi/(k_\perp\xi) \gtrsim 1$]. Let us now introduce a Fourier transformation:

$$\hat{\psi}_{\mathbf{p}} = \frac{1}{k_\perp}\int_{-\infty}^{+\infty} \hat{\psi}(s,\theta_p) e^{-iqs/\hbar} ds. \tag{17}$$

The variable s is a coordinate along a quasiclassical trajectory, which is a straight line along the direction of the quasiparticle momentum. The trajectory orientation angle is given by the θ_p value. The wave function in the real space can be found from Eqs. (15) and (17):

$$\hat{\Psi}(r,\theta) = \int_0^{2\pi} e^{ik_\perp r\cos(\theta-\theta_p)} \hat{\psi}[r\cos(\theta-\theta_p),\theta_p]\frac{d\theta_p}{2\pi}, \tag{18}$$

where (r,θ,z) is a cylindrical coordinate system. The expression for coordinate operator in (s,θ_p) representation reads:

$$\hat{\mathbf{r}} = s\mathbf{p}_0 + \frac{i}{2k_\perp}\left\{ [\mathbf{z}_0,\mathbf{p}_0], \frac{\partial}{\partial\theta_p} \right\}.$$

Then, BdG Eq. (14) in (s,θ_p) representation takes the form $\hat{H}\hat{\psi}(s,\theta_p) = \varepsilon\hat{\psi}(s,\theta_p)$ with the Hamiltonian given by

$$\hat{H} = -i\hat{\sigma}_z\frac{\hbar^2 k_\perp}{m}\frac{\partial}{\partial s} + \begin{bmatrix} 0 & \Delta(\hat{\mathbf{r}}) \\ \Delta^*(\hat{\mathbf{r}}) & 0 \end{bmatrix}, \tag{19}$$

where $\hat{\sigma}_x$, $\hat{\sigma}_y$, and $\hat{\sigma}_z$ are the Pauli matrices.

Note that the gap function operator $\Delta(\hat{\mathbf{r}})$ in Eq. (19) contains a differential operator $\partial/\partial\theta_p$, therefore the above quasiclassical equations are still rather complicated partial differential equations. A further simplification can be obtained considering eikonal approximation for the angular dependence of wave function:

$$\hat{\psi}(s,\theta_p) = e^{iS_e(\theta_p)}\hat{g}(s,\theta_p),$$

where

$$-\frac{1}{k_\perp}\frac{\partial S_e}{\partial\theta_p} = b(\theta_p),$$

is an impact parameter of a quasiclassical trajectory. Assuming that the angular dependence of $\hat{g}(s,\theta_p)$ is rather slow, one can neglect its angular derivatives in Eq. (19). The resulting Andreev equations characterizing the behavior of the wave function along a trajectory with a certain orientational angle θ_p and an impact parameter b read:

$$-i\hat{\sigma}_z\frac{\hbar^2k_\perp}{m}\frac{\partial\hat{g}}{\partial s}+\hat{\sigma}_x\,\mathrm{Re}\,\Delta(x,y)\hat{g}-\hat{\sigma}_y\,\mathrm{Im}\,\Delta(x,y)\hat{g}=\varepsilon\hat{g}, \tag{20}$$

where

$$x=s\cos\theta_p-b\sin\theta_p,$$

$$y=s\sin\theta_p+b\cos\theta_p. \tag{21}$$

Note that the Andreev Eq. (20) can be obtained directly from the initial BdG Eq. (14) if one applies the coordinate system transformation Eq. (21) and neglects the second-order derivatives of the wave function.

IV. QUASIPARTICLE SPECTRUM OF A MULTIQUANTUM VORTEX

We start our quantitative analysis of quasiparticle spectra with the case of a multiquantum vortex with vorticity M. In this section we neglect the effect of normal quasiparticle scattering at the sample boundary and focus on the peculiarities of the spectrum depending on the vorticity value. We take the gap profile in the form:

$$\Delta=D_M(r)e^{iM\theta}. \tag{22}$$

In s,θ_p variables one obtains:

$$\Delta=D_M(\sqrt{s^2+b^2})e^{iM\theta_p}\left(\frac{s+ib}{\sqrt{s^2+b^2}}\right)^M. \tag{23}$$

Due to the cylindrical symmetry, the θ_p dependence of the function $\hat{g}$ can be excluded using the gauge transformation,

$$\hat{g}=\exp(iM\hat{\sigma}_z\theta_p/2)\hat{f}, \tag{24}$$

and quasiclassical Eq. (20) takes the form,

$$-i\hat{\sigma}_z\frac{\hbar^2k_\perp}{m}\frac{\partial\hat{f}}{\partial s}+\hat{\sigma}_xG_R\hat{f}-\hat{\sigma}_yG_I\hat{f}=\varepsilon\hat{f}. \tag{25}$$

Here we introduce the functions,

$$G_R=D_M(\sqrt{s^2+b^2})\mathrm{Re}\left[\left(\frac{s+ib}{\sqrt{s^2+b^2}}\right)^M\right],$$

$$G_I=D_M(\sqrt{s^2+b^2})\mathrm{Im}\left[\left(\frac{s+ib}{\sqrt{s^2+b^2}}\right)^M\right].$$

To apply the method analogous to the one used in Ref. 8 for a singly quantized vortex, we note that the exact solutions of the above equations corresponding to $\varepsilon=0$ can be found in case $G_I\equiv 0$:

$$\hat{f}_\pm=(1,\pm i)\exp\left(\pm\frac{m}{\hbar^2k_\perp}\int_0^s G_R ds\right). \tag{26}$$

Provided G_R is an odd function of s, which tends to a certain nonzero value for $|s|\to\infty$, one of these solutions appears to decay both at negative and positive s and, thus, we get a localized wave function corresponding to a midgap bound state. Using this localized solution as a zero-order approximation for the wave function, the spectrum can be found within the first-order perturbation theory assuming that $|\varepsilon|\ll\Delta_0$.

For an arbitrary value of vorticity the function G_R is not necessary odd. In order to use the perturbation method described above we apply a gauge transformation,

$$\hat{f}=\left(\frac{s+i\hat{\sigma}_zb}{\sqrt{s^2+b^2}}\right)^\alpha\hat{w}, \tag{27}$$

so that the wave function $\hat{w}$ satisfies the following equation:

$$\left[-i\hat{\sigma}_z\frac{\hbar^2k_\perp}{m}\frac{\partial}{\partial s}+\hat{\sigma}_xG_R^{(\alpha)}-\hat{\sigma}_yG_I^{(\alpha)}+\varepsilon_d\right]\hat{w}=\varepsilon\hat{w}. \tag{28}$$

Here

$$\varepsilon_d=-\frac{\hbar^2k_\perp}{m}\frac{\alpha b}{s^2+b^2}, \tag{29}$$

is the Doppler shift, and

$$G_R^{(\alpha)}=D_M(\sqrt{s^2+b^2})\mathrm{Re}\left[\left(\frac{s+ib}{\sqrt{s^2+b^2}}\right)^{M-2\alpha}\right],$$

$$G_I^{(\alpha)}=D_M(\sqrt{s^2+b^2})\mathrm{Im}\left[\left(\frac{s+ib}{\sqrt{s^2+b^2}}\right)^{M-2\alpha}\right], \tag{30}$$

are the real and imaginary parts of the off-diagonal potential, correspondingly. One can see that choosing $M-2\alpha$ to be an odd positive integer we can change the parity of the potentials in the Hamiltonian so that $G_R^{(\alpha)}(s)$ is an odd function. Comparing Eqs. (25) and (28) we observe that the above gauge transformation also produces a Doppler shift of the energy levels. In principle, both the Doppler shift term and the term $\hat{\sigma}_yG_I^{(\alpha)}$ are not small and can be of the order of Δ_0 if the impact parameter is rather large: $b\sim\xi$. Thus, strictly speaking we can consider the expression (26) with G_R replaced by $G_R^{(\alpha)}(s)$ as a zero-order approximation and use the perturbation technique discussed above only provided that the energy corrections arising from the terms $\hat{\sigma}_yG_I^{(\alpha)}$ and ε_d almost compensate each other. For the anomalous branches, which cross the Fermi level at certain impact parameters $-\mu_j/k_\perp$, the perturbation method should be adequate in the vicinity of these points. Changing α in the interval $0\le\alpha<M/2$, we get a set of possible odd $M-2\alpha$ values providing us a set of different zero-order approximations—which allow us to obtain the spectrum as a function of b. Surprisingly, we shall see below that this method can describe the spectrum behavior even beyond its validity domain, i.e., when the energy is comparable to $\pm\Delta_0$.

It is convenient to parametrize the wave functions as

$$\hat{w}=e^{\zeta(s)}\begin{bmatrix}e^{i\eta(s)/2}\\ e^{-i\eta(s)/2}\end{bmatrix}. \tag{31}$$

As a result, we have the following equations:

$$\frac{\hbar^2k_\perp}{2m}\frac{\partial\eta}{\partial s}+G_R^{(\alpha)}\cos\eta+G_I^{(\alpha)}\sin\eta=\varepsilon-\varepsilon_d,$$

$$\frac{\hbar^2 k_\perp}{m}\frac{\partial \zeta}{\partial s} + G_R^{(\alpha)} \sin\,\eta - G_I^{(\alpha)} \cos\,\eta = 0. \tag{32}$$

Considering the localized states one should take the following boundary conditions for odd $M-2\alpha$ values:

$$\cos\,\eta(\pm\infty) = \pm\,\varepsilon/\Delta_0, \quad \sin\,\eta(\pm\infty) = \sqrt{1-\varepsilon^2/\Delta_0^2}. \tag{33}$$

In order to construct the solution we note that the mutual phase η of the electron and hole components in the zero-order solution Eq. (26) is constant $[\eta(s)=\pi/2]$. Therefore, within the perturbation theory we can linearize Eq. (32) for η close to $\pi/2$ introducing $\tilde{\eta}=\pi/2-\eta$:

$$\frac{\partial \tilde{\eta}}{\partial s} - \frac{2m}{\hbar^2 k_\perp} G_R^{(\alpha)} \tilde{\eta} = \frac{2m}{\hbar^2 k_\perp}[\varepsilon_d + G_I^{(\alpha)} - \varepsilon]. \tag{34}$$

To exclude the divergent solutions of this equation, we should impose the integral condition describing the anomalous spectral branches:

$$\varepsilon_M^{(\alpha)} = \frac{\int_0^\infty [\varepsilon_d + G_I^{(\alpha)}(s)] e^{-K(s)} ds}{\int_0^\infty e^{-K(s)} ds}, \tag{35}$$

where

$$K(s) = \frac{2m}{\hbar^2 k_\perp}\int_0^s G_R^{(\alpha)}(t)dt. \tag{36}$$

Taking $D_1(r)=\Delta_0 r/\sqrt{r^2+\xi_v^2}$ and $\alpha=0$ for the simplest case of a singly quantized vortex $(M=1)$, we get an explicit expression for the CdGM spectrum:

$$\varepsilon_1^{(0)} = \frac{\Delta_0 b}{\sqrt{b^2+\xi_v^2}} \frac{\mathcal{K}_0[2m\Delta_0\sqrt{b^2+\xi_v^2}/(\hbar^2 k_\perp)]}{\mathcal{K}_1[2m\Delta_0\sqrt{b^2+\xi_v^2}/(\hbar^2 k_\perp)]}, \tag{37}$$

where $\mathcal{K}_n$ is the McDonald function. To obtain the spectrum for $M=2$, we need to consider the case $\alpha=1/2$ so that to reduce the problem to the one for a unity vorticity and a certain Doppler shift. For the case $M=3$ the set of anomalous branches can be obtained by taking two α values: $\alpha=0$ and $\alpha=1$. The solution $\varepsilon_3^{(0)}(b)$ gives us the branch crossing the Fermi level at zero impact parameter, while two other branches are described by $\varepsilon_3^{(1)}(b)$. The typical plots of quasiparticle spectra for vortices with winding numbers $M=1,2,3$ are shown in Fig. 4. Comparing the spectra $\varepsilon_M^{(\alpha)}$ with the branches obtained from our direct numerical analysis of BdG Eq. (14), one can see that our perturbation method provides a reasonable description of the low-energy spectrum behavior. The numerical solution of the eigenvalue problem Eq. (14) was carried out using a representation of the BdG operator in the truncated basis of the normal-metal eigenfunctions. We solved the system of linear equations, which correspond to the boundary conditions at the superconductor/insulator boundary of a cylinder with a finite radius (we took $R=7\xi$). The small oscillations of the spectrum as a function of b (solid red lines in Fig. 4) resulted from the interference of incident and reflected from the boundary quasiparticle waves.[13] Note, that our perturbation procedure fails to describe proper behavior of all the branches in the vicinity of the gap value Δ_0, e.g., for $M=2$ the function $\varepsilon_2^{(1/2)}$ jumps at $b=0$ from the upper branch to the lower one and, thus, we cannot describe the part of the upper branch approaching Δ_0 for $b>0$.

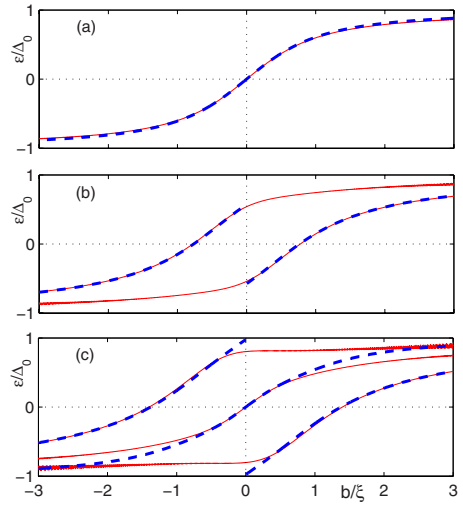

FIG. 4. (Color online) The anomalous spectral branches as functions of the impact parameter b for $k_z=0$ obtained from Eq. (35) (blue dashed lines) for (a) $M=1$, (b) $M=2$, and (c) $M=3$. The anomalous spectral branches obtained from numerical solution of the eigenvalue problem [Eq. (14)] are shown by solid red lines. The gap profiles are approximated as $D_M(r)=\Delta_0(r/\sqrt{r^2+\xi^2})^M$ with the parameter $k_F\xi=200$.

To obtain the spectrum as a function of discrete variable μ instead of a continuous b, we should apply the Bohr-Sommerfeld quantization rule for the angular momentum [see Eq. (8)] with $\beta=\{M/2\}$, which results from the obvious condition that the wave function $\hat{g}$ is single valued. Here $\{\ldots\}$ denotes the fractional part. For the odd (even) vorticity M we obtain $\mu=n+1/2$ $(\mu=n)$, where n is an integer.

V. DECAY OF A MULTIQUANTUM VORTEX INTO A SET OF SEPARATED VORTICES

In this section we consider modification of the quasiparticle spectrum caused by the decay of a multiquantum vortex into a set of separated singly quantized vortices, which occurs under the decreasing magnetic field. For simplicity sake we restrict ourselves to the case of a two-vortex system with a certain intervortex distance a controlled by the external magnetic field. The case $a=0$ corresponds to a doubly quantized vortex while the limit $a \gg \xi$ corresponds to a pair of isolated singly quantized vortices. In this section we again neglect the effect of normal quasiparticle scattering at the sample boundary.

A. Quasiclassical consideration

As a first step of our analysis we choose to apply the approximate quasiclassical procedure developed in the previous section. It is natural to expect that the validity range for this method should be restricted to the region of rather

small distances $a<a_c$ when one can neglect the Landau-Zener tunneling between the quasiclassical orbits $\mu(\theta_p)$ described in Sec. II. To describe the system of two singly quantized vortices positioned at $\mathbf{r}=\pm\mathbf{a}/2=\pm(a/2,0)$, we fit the gap function as follows:

$$\Delta(\mathbf{r}) = \Delta_0 f_1\left(\mathbf{r}-\frac{\mathbf{a}}{2}\right) f_1\left(\mathbf{r}+\frac{\mathbf{a}}{2}\right) = \Delta_0 \left|f_1\left(\mathbf{r}-\frac{\mathbf{a}}{2}\right)\right| \left|f_1\left(\mathbf{r}+\frac{\mathbf{a}}{2}\right)\right| \times \frac{x+iy-\frac{a}{2}}{\left|x+iy-\frac{a}{2}\right|} \frac{x+iy+\frac{a}{2}}{\left|x+iy+\frac{a}{2}\right|}, \tag{38}$$

where $f_1(\mathbf{r})$ is a normalized gap function of a singly quantized vortex. It is convenient to rewrite the above expression as a superposition of functions with two different vorticities:

$$\Delta(\mathbf{r}) = \Delta_0[f_2(\mathbf{r})e^{2i\theta} + f_0(\mathbf{r})]. \tag{39}$$

Taking the simplest core model,

$$|f_1(\mathbf{r})| = \frac{r}{\sqrt{r^2+\xi_v^2}}, \tag{40}$$

with the core size ξ_v, we obtain

$$f_2(\mathbf{r}) = \frac{x^2+y^2}{\sqrt{\left(x^2+y^2+\xi_v^2+\frac{a^2}{4}\right)^2 - a^2x^2}},$$

$$f_0(\mathbf{r}) = -\frac{\frac{a^2}{4}}{\sqrt{\left(x^2+y^2+\xi_v^2+\frac{a^2}{4}\right)^2 - a^2x^2}}.$$

To solve Eq. (20) with the gap function given by Eq. (39), we apply the gauge transformation Eq. (27) with $\alpha=1/2$. The expression for the quasiclassical spectrum takes Eq. (35) with

$$G_R = \Delta_0\left[f_2(x,y)\frac{s}{\sqrt{s^2+b^2}} + f_0(x,y)\frac{s\cos(2\theta_p) - b\sin(2\theta_p)}{\sqrt{s^2+b^2}}\right], \tag{41}$$

$$G_I = \Delta_0\left[f_2(x,y)\frac{b}{\sqrt{s^2+b^2}} + f_0(x,y)\frac{s\sin(2\theta_p) + b\cos(2\theta_p)}{\sqrt{s^2+b^2}}\right], \tag{42}$$

where (x,y) variables are given by Eq. (21).

The resulting dependencies of the impact parameter vs θ_p for zero energy and different intervortex distances are shown in Fig. 5. These calculations of the low-energy part of the spectrum appear to be in good agreement with the two-level model Eq. (4) and, thus, the angular dependence of the impact parameter can be fitted by the expression:

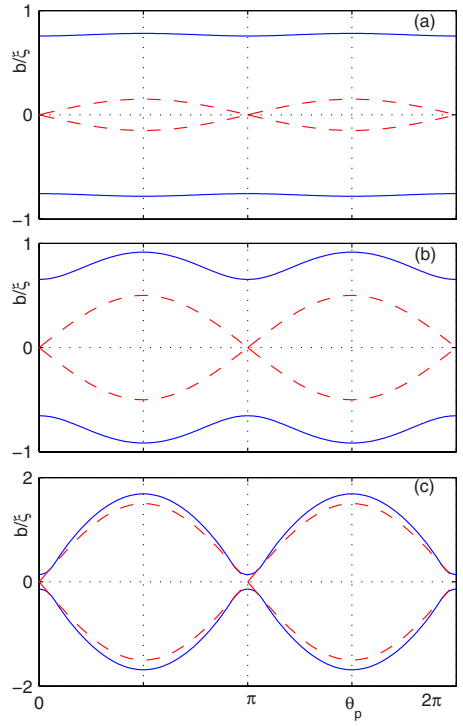

FIG. 5. (Color online) The isoenergetic curves $b(\theta_p)$ for a two-vortex system. We choose here (a) $\varepsilon=0$, $k_z=0$, and $a=0.3\xi$; (b) $a=\xi$; and (c) $a=3\xi$. The dashed curves correspond to the isoenergetic lines for two noninteracting singly quantized vortices. The gap is approximated by Eqs. (38) and (40) with $\xi_v=\xi$.

$$b(\theta_p) = \frac{\varepsilon}{\tilde{\omega}(k_z,a)k_\perp} \pm \sqrt{\tilde{b}^2(k_z,a) + \left(\frac{a}{2}\sin\theta_p\right)^2}, \tag{43}$$

where $\tilde{\omega}(k_z,a)\sim\Delta_0/k_\perp\xi$ and $\tilde{b}=\delta\varepsilon/(k_\perp\omega)$ is the splitting of quasiclassical orbits. In the limit $a=0$ we get the spectrum of a doubly quantized vortex: $\varepsilon=\tilde{\omega}(k_z,0)[b\pm\tilde{b}(k_z,0)]$, where $\tilde{b}(k_z,0)$ is of the order of ξ for small k_z values. For large intervortex distances the value $\tilde{b}$ is exponentially small: $\tilde{b}\sim\xi\exp[-k_Fa/(k_\perp\xi)]$ [see Eq. (5)]. Generally, in the whole interval of distances a the splitting of quasiclassical orbits is defined by the overlapping of the wave functions localized in the cores of neighboring singly quantized vortices. This overlapping is determined by the factor $\exp[-K_0(s)]$ describing the decay of the wave function in a singly quantized vortex (see Ref. 6):

$$K_0(s) = \frac{2m}{\hbar^2k_\perp}\int_0^s \Delta(t)dt. \tag{44}$$

Thus, the spectrum Eq. (35) can be fitted by the one describing the two-level system if we put $\tilde{b}=\tilde{b}(k_z,0)\times\exp[-K_0(a/2)]$. Taking the vortex core model Eq. (40), we obtain:

$$\tilde{b} = \tilde{b}(k_z,0)\exp\left[-2\frac{k_F}{k_\perp}\frac{\xi_v}{\xi}\left(\sqrt{\frac{a^2}{4\xi_v^2}+1}-1\right)\right]. \tag{45}$$

Comparing this approximate expression with the orbit splitting calculated using the spectrum Eq. (35) (see Fig. 6 for the

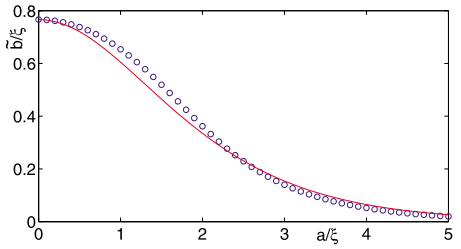

FIG. 6. (Color online) Splitting of quasiclassical orbits $\tilde{b}$ obtained from Eq. (45) (solid line) and found from the spectrum of a two-vortex system Eq. (35) (circles) for $k_z=0$. The gap profile is approximated by Eq. (39) with $\xi_v=\xi$.

particular case $k_z=0$), we can find appropriate $\tilde{b}(k_z,0)$ values.

To find the quantized energy levels, we can use the Bohr-Sommerfeld quantization rule [Eq. (8)]—which takes the form $S(\varepsilon,k_z)=2\pi(n+\beta)$, where

$$S(\varepsilon,k_z)=\int_0^{2\pi}\mu(\theta_p)d\theta_p=-k_\perp\int_0^{2\pi}b(\theta_p)d\theta_p, \qquad (46)$$

is the area under the isoenergetic line $\mu(\varepsilon,k_z)$ in the (μ,θ_p) plane. Calculating this integral for the two-level model [Eq. (43)], we obtain

$$S(\varepsilon,k_z)=-2\pi\frac{\varepsilon}{\tilde{\omega}}\pm 2k_\perp\sqrt{a^2+4\tilde{b}^2}E\left(\frac{a}{\sqrt{a^2+4\tilde{b}^2}}\right), \quad (47)$$

where $E(k)=\int_0^{\pi/2}\sqrt{1-k^2\sin^2\theta}d\theta$ is the complete elliptic integral of the second type. As a result, we find the quasiparticle spectrum of a two-vortex system,

$$\varepsilon_n=\tilde{\omega}\left[-n-\beta\pm\frac{k_\perp\sqrt{a^2+4\tilde{b}^2}}{\pi}\mathrm{E}\left(\frac{a}{\sqrt{a^2+4\tilde{b}^2}}\right)\right]. \qquad (48)$$

The spectrum Eq. (48) is analogous to the spectrum of the doubly quantized vortex Eq. (1) and is drastically different from the CdGM spectrum. The case $a=0$ gives us the spectrum Eq. (1) of a doubly–quantized vortex. Treating the opposite limit $a\gg\tilde{b}$ with the logarithmic accuracy, we obtain

$$S(\varepsilon,k_z)=-2\pi\frac{\varepsilon}{\tilde{\omega}}\pm 2k_\perp a\left[1+2\left(\frac{\tilde{b}}{a}\right)^2\ln\left(\frac{a}{\tilde{b}}\right)\right], \quad (49)$$

and

$$\varepsilon_n=\tilde{\omega}\left\{-n\pm\frac{k_\perp a}{\pi}\left[1+2\left(\frac{\tilde{b}}{a}\right)^2\ln\left(\frac{a}{\tilde{b}}\right)\right]\right\}. \qquad (50)$$

B. Landau-Zener tunneling between quasiclassical orbits

The above description is valid provided the intervortex distance is rather small ($a<a_c$) when the splitting $\delta\mu$ between isoenergetic lines $\mu(\theta_p)$ is large compared to the quantum-mechanical uncertainty of the angular momentum $\Delta\mu$ and the probability of the Landau-Zener tunneling between quasiclassical orbits can be neglected [see Eq. (7)]. As a next step, we proceed with a quantitative analysis of quasiparticle spectrum of the two-vortex system in case of the small splitting of the isoenergetic lines in (μ,θ_p) plane when the vortices are well separated so that $a\gtrsim a_c$. In order to calculate the quasiparticle spectrum taking into account the influence of Landau-Zener tunneling, we should go beyond the quasiclassical consideration of the angular precession of quasiparticle trajectories. It means that we cannot neglect the noncommutativity of canonical variables: $[\hat{\mu},\theta_p]=-i$, where θ_p is the trajectory orientation angle and $\hat{\mu}=-i\partial/\partial\theta_p$ is the angular momentum operator. Keeping in mind the symmetry of the gap function in a two-vortex system, we can reduce the problem to the one describing a single vortex with an additional boundary condition imposed on the wave function at the plane $x=0$ positioned between vortices. Indeed, the gap function distribution corresponding to the two-vortex system possesses the following symmetry: $\Delta(x,y)=\Delta^*(-x,y)$. As a result, for the eigenfunctions we obtain

$$\hat{\Psi}(x,y)=e^{i\chi}\hat{\Psi}^*(-x,y), \qquad (51)$$

where χ is a constant phase. The spectrum does not depend on χ since for any eigenfunction $\hat{\Psi}$ satisfying Eq. (51) we can introduce a new function $\hat{\Psi}_1=\hat{\Psi}e^{-i\chi/2}$, which corresponds to the same energy level and has the following symmetry: $\hat{\Psi}_1(x,y)=\hat{\Psi}_1^*(-x,y)$. Therefore we can choose $\chi=0$ and obtain the boundary conditions at the plane $x=0$:

$$\hat{\Psi}=\hat{\Psi}^*;\quad \frac{\partial\hat{\Psi}}{\partial x}=-\frac{\partial\hat{\Psi}^*}{\partial x}. \qquad (52)$$

For the sake of simplicity we neglect the anisotropy of the gap function around the vortex positioned in the half space $x<0$. Nevertheless the solution cannot be characterized by a definite angular momentum because of the above boundary condition responsible for interaction of different angular harmonics. Thus, following Ref. 14 we introduce the angular momentum expansion for the solution:

$$\hat{\psi}(s,\theta_p)=\sum_\mu e^{i\mu\theta_p+i\hat{\sigma}_z\theta_p/2}\hat{g}_\mu(s), \qquad (53)$$

where $\mu=n+1/2$ and n is an integer. The function $\hat{g}_\mu$ satisfies the Andreev Eq. (20) along the quasiclassical trajectory with $b=-\mu/k_\perp$. For small impact parameters $b\ll\xi$ Eq. (20) can be solved analytically, yielding a general expression for the function $\hat{g}_\mu(s)$ in the following form:

$$\hat{g}_\mu(s)=c_\mu\hat{G}_{1\mu}(s)+d_\mu\hat{G}_{2\mu}(s),$$

where c_μ and d_μ are arbitrary constants. We choose the fundamental solutions so that $G_{1\mu}(-\infty)=0$ while $G_{2\mu}(+\infty)=0$ (see Ref. 14):

$$\hat{G}_{1\mu}=\left[e^{-|K_0(s)|/2}-i\frac{\gamma}{2}(\mathrm{sgn}\ s+1)\hat{\sigma}_z e^{|K_0(s)|/2}\right]\hat{\lambda},$$

$$\hat{G}_{2\mu} = \left[e^{-|K_0(s)|/2} - i\frac{\gamma}{2}(\mathrm{sgn}\, s - 1)\hat{\sigma}_z e^{|K_0(s)|/2} \right]\hat{\lambda}.$$

Here $\hat{\lambda} = [\exp(i\pi/4), \exp(-i\pi/4)]$,

$$\gamma(\mu) = \frac{\Lambda}{\Delta_0}[\varepsilon(\mu) - \varepsilon], \tag{54}$$

$$\Lambda = \frac{2k_F}{k_\perp \xi}\int_0^\infty e^{-K_0(s)} ds. \tag{55}$$

Here the CdGM spectrum is taken as a linear function of $|\mu|$ for small $\mu \ll k_\perp \xi_v$: $\varepsilon(\mu) = -\mu\omega$, with interlevel spacing

$$\omega = \frac{1}{\Lambda}\frac{2k_F}{k_\perp^2 \xi}\int_0^\infty \frac{\Delta(s)}{s} e^{-K_0(s)} ds.$$

It is convenient to introduce the angle dependent functions:

$$C(\theta_p) = \sum_\mu e^{i\mu\theta_p} c_\mu, \quad D(\theta_p) = \sum_\mu e^{i\mu(\theta_p + \pi)} d_\mu.$$

These functions appear to be nonzero only in the angular interval $-\pi/2 < \theta_p < \pi/2$ because of the decay of the wave function $\hat{\Psi}(x,y)$ in the left half space far from the vortex. At the boundaries of this angular interval we should impose the conditions,

$$C(\pm\pi/2) = \pm D(\mp\pi/2), \tag{56}$$

which result from the continuity of the wave function $\psi(s,\theta_p)$.

Within the large-angle domain $|\theta_p| \gg \xi/a$ the wave function $\hat{\psi}(s,\theta_p)$ can be found using a tight-binding approximation as a sum of two single vortex solutions localized on vortices at $\mathbf{r} = \pm(a/2, 0)$ (see Ref. 7). Comparing the tight-binding solution with Eq. (53), we obtain that $\Sigma\gamma(\mu) e^{i\theta_p\mu} c_\mu = 0$ and $\Sigma\gamma(\mu) e^{i(\theta_p+\pi)\mu} d_\mu = 0$, or

$$C(\theta_p), D(\theta_p - \pi) \sim e^{-i\varepsilon\theta_p/\omega}. \tag{57}$$

The deviations of angular functions $C(\theta_p)$ and $D(\theta_p)$ from Eq. (57) due to the intervortex quasiparticle tunneling occur in the narrow angular domain $|\theta_p| \ll \xi/a$. Within this domain we apply the stationary phase method to handle the integral in Eq. (18). For a given value of angular momentum μ the stationary phase points are given by $\sin(\theta_p - \theta) = \mu/[k_\perp R(\theta)]$, where $R(\theta) = a/(2\cos\theta)$ corresponds to the line $x = 0$ in the polar coordinate system with the origin in the vortex center. Assuming $|\mu| \ll k_\perp a$ and $|\theta| \ll \pi$, we obtain the stationary phase points: $\theta_{p1} \approx \theta + 2\mu/(k_\perp a)$ and $\theta_{p2} = \pi + \theta - 2\mu/(k_\perp a)$. Then, the expression for the wave function $\Psi(r,\theta)$ at $r = R(\theta)$ and $|\theta| \ll \pi$ reads as follows:

$$\hat{\Psi}[R(\theta),\theta] = e^{i\varphi}\int_{-\infty}^{\infty} e^{i\mu^2/k_\perp a}[e^{-K_0(a/2)} - i\gamma\hat{\sigma}_z]\hat{\lambda} e^{i\mu\theta} c_\mu d\mu$$

$$- \hat{\sigma}_z e^{-i\varphi}\int_{-\infty}^{\infty} e^{-i\mu^2/k_\perp a}[e^{-K_0(a/2)}$$

$$+ i\gamma\hat{\sigma}_z]\hat{\lambda} e^{i\mu(\theta+\pi)} d_\mu d\mu,$$

where $\varphi = k_\perp a(1 + \theta^2/2)/2$ and the discreteness of angular momentum μ is neglected. Then, from Eq. (52) we obtain

$$\mathrm{Im}\left\{ e^{i\varphi}\int_{-\infty}^{\infty} e^{i\mu^2/k_\perp a}[e^{-K_0(a/2)} - i\gamma\hat{\sigma}_z]\hat{\lambda} e^{i\mu\theta} c_\mu d\mu \right\} = 0, \tag{58}$$

which yields the following equation (see Appendix A):

$$[e^{-K_0(a/2)} - i\hat{\sigma}_z\hat{\gamma}]\hat{\lambda} C_2(\theta) = e^{-2i\tilde{\varphi}}[e^{-K_0(a/2)} + i\hat{\sigma}_z\hat{\gamma}]\hat{\lambda}^* C_1(\theta), \tag{59}$$

where $\tilde{\varphi} = k_\perp a(1 - \theta^2/2)/2$, $C_2(\theta) = iC(\theta)$, and $C_1(\theta) = C^*(-\theta)$. Then, Eq. (59) can be written as follows:

$$\left(i\omega\frac{\partial}{\partial\theta} - \varepsilon \right) C_2(\theta) = e^{-2i\tilde{\varphi}} J C_1(\theta),$$

$$\left(i\omega\frac{\partial}{\partial\theta} - \varepsilon \right) C_1(\theta) = e^{2i\tilde{\varphi}} J C_2(\theta), \tag{60}$$

where the overlap integral is

$$J = \frac{\Delta_0}{\Lambda} e^{-K_0(a/2)}. \tag{61}$$

Analogously, for the functions $D_2(\theta) = iD(\theta)$ and $D_1(\theta) = D^*(-\theta)$ we obtain

$$\left(i\omega\frac{\partial}{\partial\theta} - \varepsilon \right) D_2(\theta) = e^{2i\tilde{\varphi}} J D_1(\theta),$$

$$\left(i\omega\frac{\partial}{\partial\theta} - \varepsilon \right) D_1(\theta) = e^{-2i\tilde{\varphi}} J D_2(\theta). \tag{62}$$

Considering Eqs. (60) and (62) in the angular domain $(\xi/a) \gg |\theta| \gg (\xi/a)J/\Delta_0$, we can neglect the rapidly oscillating right-hand side, therefore the asymptotic form of angular functions **C** and **D** corresponds to the noninteracting vortices:

$$\mathbf{C} = (C_1, C_2) = e^{-i\varepsilon\theta/\omega}(\tilde{c}_1, \tilde{c}_2),$$

$$\mathbf{D} = (D_1, D_2) = e^{-i\varepsilon\theta/\omega}(\tilde{d}_1, \tilde{d}_2), \tag{63}$$

where $\tilde{c}_1$, $\tilde{c}_2$, $\tilde{d}_1$, and $\tilde{d}_2$ are the arbitrary constants. Then, solving Eqs. (60) and (62) we can find the transfer matrix $\hat{X}$ matching the large-angle asymptotics:

$$\mathbf{C}(\theta_{\mathrm{th}}) = \hat{X}\mathbf{C}(-\theta_{\mathrm{th}}),$$

where $\hat{X}$ is a transfer matrix and $\theta_{\mathrm{th}} \sim \xi/a$ is a threshold angle where we match the solutions for the large-angle and small-angle domains. Introducing new functions,

$$B_2(\theta) = C_2(\theta) e^{i\tilde{\varphi} - i\varepsilon\theta/\omega}, \quad B_1(\theta) = C_1(\theta) e^{-i\tilde{\varphi} - i\varepsilon\theta/\omega},$$

we obtain the following equations:

$$\left(i\frac{\partial}{\partial\tilde{\theta}} + \tilde{\theta} \right) B_1 = pB_2,$$

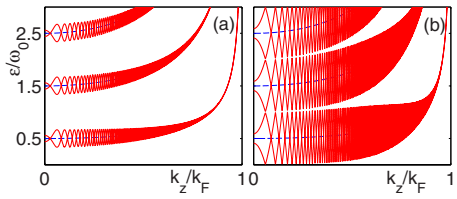

FIG. 7. (Color online) The quasiparticle spectrum of two vortices calculated using the Eq. (68) for (a) $a=5\xi$ and (b) $a=3.5\xi$. The CdGM spectrum is shown by the dashed lines. The vortex core profile for a single vortex is approximated by Eq. (40) with $\xi_v=\xi$ and $k_F\xi=200$.

$$\left(i\frac{\partial}{\partial\tilde{\theta}}-\tilde{\theta}\right)B_2=pB_1, \tag{64}$$

where

$$p=\frac{J}{\omega\sqrt{k_\perp a/2}}, \tag{65}$$

and $\tilde{\theta}=\theta\sqrt{k_\perp a/2}$. This equations coincide with equations obtained in Ref. 7. The problem described by the Eq. (64) is equivalent to the one describing the interband tunneling[18] or the one-dimensional motion of a Dirac particle in a uniform electric field and the solution can be written in terms of the parabolic cylinder functions (see Appendix B), yielding the transfer matrix,

$$\hat{X}=e^{-\pi p^2/2}\hat{I}+i(\hat{\sigma}_y \text{ Re } \tau+\hat{\sigma}_x \text{ Im } \tau). \tag{66}$$

Here $\hat{I}$ is the unity matrix,

$$\tau=\sqrt{2\sinh(\pi p^2/2)}e^{-\pi p^2/4}e^{i\chi},$$

$$\chi=k_\perp a+p^2\ln(\theta_{\text{th}}\sqrt{k_\perp a})+\arg\left[\Gamma\left(1-i\frac{p^2}{2}\right)\right]+\frac{\pi}{4}, \tag{67}$$

and Γ is the gamma function. Analogously, for the functions $\mathbf{D}(\theta)$ we find,

$$\mathbf{D}(\theta_{\text{th}})=\hat{\sigma}_x\hat{X}\hat{\sigma}_x\mathbf{D}(-\theta_{\text{th}}).$$

Matching the wave function in different angular domains and using the boundary conditions Eq. (56), we obtain the spectrum,

$$\cos(\pi\varepsilon/\omega)=\pm e^{-\pi p^2/4}\sqrt{2\sinh(\pi p^2/2)}\sin\chi. \tag{68}$$

Within the present theory we cannot determine the threshold angle θ_{th} precisely. However, since the dependence of χ on θ_{th} is logarithmic, the θ_{th}-dependent term in Eq. (67) can be considered as an additional constant phase of the oscillations of the energy levels. The spectrum of two vortices calculated using Eq. (68) for small ($a>a_c$) and large ($a<a_c$) intervortex distance is shown in Fig. 7. One can see that the transformation of the spectrum $\varepsilon(k_z)$ occurs according to the scenario suggested above: as we decrease the distance a below a_c the crossover to the spectrum of the doubly quantized vortex starts in the region of small k_z values defined by the condition $p>1$. For $p\ll 1$ we get the CdGM spectrum with a small oscillatory correction:

$$\varepsilon\simeq\omega\left[n+\frac{1}{2}\mp(-1)^n(p/\sqrt{\pi})\sin\left(k_\perp a+\frac{\pi}{4}\right)\right]. \tag{69}$$

The minigap $\varepsilon_{\text{min}}=[1-2p/\sqrt{\pi}]\omega_0/2$ vanishes for $a=a_c$.

For the large values $p\gg 1$ Eq. (68) yields the spectrum in the form:

$$\varepsilon=\omega\left[n\pm\frac{k_\perp a+p^2\ln(\theta_{\text{th}}\sqrt{k_\perp a/p^2})}{\pi}\right]. \tag{70}$$

Here we have used the asymptotic formula for the argument of gamma function at $p\gg 1$: $\arg[\Gamma(1-ip^2/2)]\approx-(p^2/2)[\ln(p^2/2)-1]$. This result can be formulated as the Bohr-Sommerfeld quantization rule $S(\varepsilon,k_z)=2\pi n$ with

$$S(\varepsilon,k_z)=2\pi\frac{\varepsilon}{\omega}\pm\left[2k_\perp a+2p^2\ln\left(\theta_{\text{th}}\sqrt{\frac{k_\perp a}{|p|^2}}\right)\right]. \tag{71}$$

This result coincides with formula (49) obtained by the evaluation of the Bohr-Sommerfeld integral at quasiclassical orbits $\mu(\theta_p)$ such as the ones shown in Fig. 2(b).

VI. BOUNDARY EFFECTS: VORTEX NEAR THE SURFACE

Now we proceed with a quantitative analysis of the effect of normal reflection of quasiparticles at the boundary. We consider a vortex near a smooth surface approximated by a parabolic cylinder (see Sec. II B). Considering the quasiclassical trajectories, which are rather far from being parallel to the system optical axis, we find that either incident or reflected trajectories appears to pass far from the vortex core. The quasiclassical spectrum for this case is the same as for a single vortex:

$$\varepsilon(b,\theta_p,k_z)=-\omega k_\perp(b-d\sin\theta_p). \tag{72}$$

This spectrum should be strongly disturbed for trajectories passing close to the optical axis when both the incident and reflected trajectories pass through the vortex core. In this case the trajectory orientation angles should be taken in the domains $|\theta_p|<\xi/d$ or $|\pi-\theta_p|<\xi/d$, and the impact parameters defined relative to the point with coordinates $r=d$ and $\theta=0$ (see Sec. II B for notations) should be rather small: $|b|\ll d$. Solving Eq. (20) along the incident and reflected trajectories and matching the solutions to meet the zero boundary condition for the wave function at the surface, we obtain the quasiclassical spectrum for $|b|\ll d$ and $|\theta_p|\ll 1$;

$$\varepsilon(b,\theta_p,k_z)=-\frac{\omega k_\perp[(1+h)b+2\theta_p d]}{2}\pm\sqrt{\frac{(\omega k_\perp)^2(1-h)^2b^2}{4}+J^2}. \tag{73}$$

This expression for the quasiclassical spectrum can also be applied for the angular interval $|\theta_p-\pi|\ll 1$ provided that we replace the angle $\theta_p\to\pi-\theta_p$.

Equations (72) and (73) allow us to determine the form of isoenergetic lines $\mu(\theta_p)=-k_\perp b(\theta_p)$. Generally, one can dis-

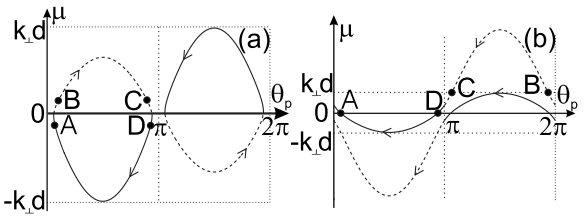

FIG. 8. The schematic plot of isoenergetic lines $\mu(\theta_p)$ corresponding to the energy $\varepsilon=0$ for a vortex near the parabolic boundary positioned at $d>|F|$: (a) $F<0$ and $h<0$; (b) $F>0, h>0$. The solid lines correspond to the trajectories passing close to the vortex core. The dashed lines represent the mapping of solid lines due to the normal reflection of trajectories at the boundary.

tinguish two types of the isoenergetic lines behavior near the points $\theta_p=\pi n$ according to the sign of the parameter $h=-(1+d/F)$. If $h<0$ (i.e., if $F>0$ or $F<0$ and $d<|F|$) there appears a prohibited angular domain with the width $\delta\theta_p=\tilde{p}/\sqrt{|\rho|}$ [Fig. 8(a)], where

$$\tilde{p}=\frac{J}{\omega\sqrt{|h\rho|}},$$

$$\rho=k_\perp d\frac{F+d/2}{F+d}. \tag{74}$$

On the other hand, for $h>0$ ($F<0$ and $d>|F|$) there appears a gap between isoenergetic lines and the prohibited angular domain disappears [Fig. 8(b)].

Solid curves in Fig. 8 correspond to the trajectories, which always pass through the vortex core. The reflection of trajectories at the boundary determines the mapping of a solid curve on the dashed curve. To determine the spectrum, we should apply the Bohr-Sommerfeld quantization rule to the closed path in (μ,θ_p) space corresponding to the precession of the trajectory around the vortex core. Let us study the formation of such closed path. We start from the consideration of the trajectory on the solid line, precessing along the orbit in the direction showed by the arrow in Fig. 8. Starting from the point D the trajectory precesses along the solid curve to point A, while the trajectory on the dashed curve moves from point B toward point C. As the incident trajectory goes from point A on the solid curve to point B on the dashed curve, the corresponding reflected trajectory goes from point C on the dashed curve to point D on the solid curve. Thus, the trajectory is reflected from the boundary and appears at point D again. Therefore the quasiclassical orbit in Fig. 8 forms a closed path since the quasiparticle states in points A and D are identical. Now we can apply the Bohr-Sommerfeld quantization rule for the closed orbits in Fig. 8: $S(\varepsilon,k_z)=2\pi n$, where n is an integer and $S(\varepsilon,k_z)$ is the area under the solid curves $\mu(\theta_p)$ in Fig. 8, taken in the angle domains $0<\theta_p<\pi$ and $\pi<\theta_p<2\pi$. Evaluating the integral, we obtain

$$S(\varepsilon,k_z)=-\pi\frac{\varepsilon}{\omega_s}\pm\left[2k_\perp d+\mathrm{sgn}(h)\tilde{p}^2\ln\left(\theta_{\mathrm{th}}\sqrt{\frac{|\rho|}{\tilde{p}^2}}\right)\right], \tag{75}$$

where the interlevel spacing is

$$\omega_s=\omega\left[1+\mathrm{sgn}(h)\frac{1}{\pi\theta_{\mathrm{th}}}\frac{\tilde{p}^2}{k_\perp d}\right]^{-1}. \tag{76}$$

The threshold angle θ_{th} is of the order of $\xi/(2d)$.

By increasing the distance from the vortex to the surface, the splitting of the isoenergetic lines tends to be zero. According to the arguments presented in Sec. II the probability of the tunneling between different quasiclassical orbits can be estimated as follows [see Eq. (13)]: $W\sim\exp[-2\pi(\delta\theta_p/\Delta\theta_p)^2]$, where $\delta\theta_p=\tilde{p}/\sqrt{|\rho|}$ and $\Delta\theta_p\sim 1/\sqrt{|\rho|}$. When the splitting is so small that $W\sim 1$ (if $\tilde{p}\ll 1$), the above consideration becomes insufficient and we should take into account the Landau-Zener transitions between the quasiclassical orbits.

To study this limit, we employ the approach developed in Sec. V B. The wave functions should vanish at the sample surface,

$$\int_0^{2\pi}e^{ik_\perp R(\theta)\cos(\theta_p-\theta)}\hat{\psi}[R(\theta)\cos(\theta_p-\theta),\theta_p]d\theta_p=0. \tag{77}$$

Using the same technique as in Sec. V B, we obtain

$$\left(i\omega\frac{\partial}{\partial\theta}-\varepsilon\right)C_1(\theta)=e^{i\rho\theta^2-2ik_\perp d}\frac{J}{\sqrt{h}}C_2(\theta),$$

$$\left(i\omega\frac{\partial}{\partial\theta}-\frac{\varepsilon}{h}\right)C_2(\theta)=e^{-i\rho\theta^2+2ik_\perp d}\frac{J}{\sqrt{h}}C_1(\theta), \tag{78}$$

where $C_1(\theta)=C(\theta)$ and $C_2(\theta)=iD(\theta/h)$. The boundary conditions for $C_{1,2}(\theta)$ are:

$$iC_2(h\pi/2)=C_1(-\pi/2),$$

$$iC_1(\pi/2)=C_2(-h\pi/2). \tag{79}$$

It is important to notice that Eq. (78) is valid until $k_\perp d|h|\gg 1$. Since the case $h=0$ correspond to the vortex positioned at the focal point of a concave surface, the above condition means that the vortex distance from the focal point is much larger than the atomic scale. In case when the vortex is situated at the center of the surface curvature ($d=-2F$, $h=1$, and $\rho=0$) Eq. (78) appears to be very similar to Eq. (15) of Ref. 14 obtained for a vortex at the center of a superconducting disk. The only difference is caused by the absence of the quasiparticle scattering at the opposite end of the trajectory since we assume the half-infinite superconducting sample. Hereafter considering the concave surface we focus on the case when the vortex is shifted from the curvature center toward the boundary at the distance exceeding the atomic length scale: $|\rho|\gg 1$. Then, at large angles $\theta\gg J/(\omega\sqrt{|h|}\rho)$ the rapidly oscillating right-hand side of Eq. (78) can be neglected, and we obtain the solution corresponding to the case of a single vortex in a bulk superconductor;

$$\mathbf{C} = (C_1, C_2) = (a_1 e^{-i\varepsilon\theta/\omega}, a_2 e^{-i\varepsilon\theta/\omega h}), \tag{80}$$

where a_1 and a_2 are the arbitrary constants. In order to obtain the transfer matrix $\hat{X}$ in the equation $\mathbf{C}(\theta_{\text{th}}) = \hat{X}\mathbf{C}(-\theta_{\text{th}})$ we need to consider the domain of small angles. Introducing new functions,

$$B_1(\theta) = C_1(\theta) e^{ik_\perp d} e^{-i\rho\theta^2/2 - i\varepsilon_1\theta/\omega},$$

$$B_2(\theta) = -\operatorname{sgn}(\rho) C_2(\theta) e^{-ik_\perp d} e^{i\rho\theta^2/2 - i\varepsilon_1\theta/\omega},$$

where $\varepsilon_1 = \varepsilon(h+1)/(2h)$, and a new coordinate $\tilde{\theta} = \sqrt{-\rho}(\theta + \theta_0)$ with $\theta_0 = \varepsilon(h-1)/(2\rho h\omega)$, we obtain the system of equations for $B_1(\tilde{\theta})$ and $B_2(\tilde{\theta})$. This system coincides with Eq. (64) although for $h<0$ the coordinate x is imaginary and Eq. (64) should be solved along the imaginary axis. Using the solution of Eq. (64) (see Appendix B), we obtain the transfer matrix for $h>0$;

$$\hat{X} = e^{-\pi\tilde{p}^2/2}\hat{I} - i(\hat{\sigma}_x \operatorname{Im}\tau_1 + \hat{\sigma}_y \operatorname{Re}\tau_1), \tag{81}$$

where $\hat{I}$ is the unity matrix,

$$\tau_1 = \sqrt{2\sinh(\pi\tilde{p}^2/2)}\, e^{-\pi\tilde{p}^2/4} e^{i\chi_1},$$

and $\chi_1 = 2k_\perp d + \tilde{p}^2 \ln|\tilde{\theta}^*| + \arg[\Gamma(1 - i\tilde{p}^2/2)] + \pi/4$. Analogously, for $h<0$ we get

$$\hat{X} = e^{\pi\tilde{p}^2/2}\hat{I} - (\hat{\sigma}_y \operatorname{Re}\tau_2 + \hat{\sigma}_x \operatorname{Im}\tau_2), \tag{82}$$

where

$$\tau_2 = \sqrt{2\sinh(\pi\tilde{p}^2/2)}\, e^{\pi\tilde{p}^2/4} e^{i\chi_2},$$

and $\chi_2 = 2k_\perp d - \tilde{p}^2 \ln|\tilde{\theta}^*| - \arg[\Gamma(1 - i\tilde{p}^2/2)] + \pi/4$. We denote here $\tilde{\theta}^* = \sqrt{|\rho|}(\theta_{\text{th}} + \theta_0)$.

The quasiparticle spectrum is obtained by matching the solutions in different angular domains using the transfer matrices Eqs. (81) and (82) and imposing the boundary conditions [Eq. (79)];

$$\cos\left(\frac{\pi\varepsilon}{\omega}\right) = -\operatorname{sgn}(h)\sqrt{2\sinh\left(\frac{\pi\tilde{p}^2}{2}\right)}\, e^{-\pi\tilde{p}^2/4} \operatorname{LI}\sin\chi, \tag{83}$$

where

$$\chi = 2k_\perp d + \operatorname{sgn}(h)\left\{\tilde{p}^2 \ln\left|\sqrt{|\rho|}(\theta_{\text{th}} + \theta_0)\right| + \arg\left[\Gamma\left(1 - \frac{i\tilde{p}^2}{2}\right)\right] + \frac{\pi}{4}\right\}. \tag{84}$$

The energy ε enters both the left-hand and right-hand sides [via $\theta_0 = \varepsilon(h-1)/(2\rho h\omega)$] of Eq. (83). For small energy ($|\varepsilon| \ll \Delta_0$) we have $\theta_{\text{th}} \gg \theta_0$, and the logarithm in Eq. (84) can be expanded as follows: $\ln(|\theta_{\text{th}} + \theta_0|\sqrt{|\rho|}) \approx \ln(\theta_{\text{th}}\sqrt{|\rho|}) - \theta_0/\theta_{\text{th}}$. The Landau-Zener transitions between quasiclassical orbits are important for $\tilde{p} \lesssim 1$ and, therefore, in this limit the energy dependent term in χ can always be neglected: $\tilde{p}^2\theta_0/\theta_{\text{th}} \ll 1$. In the opposite limit the probability of Landau-Zener transitions vanishes and Eq. (83) yields the spectrum in the form:

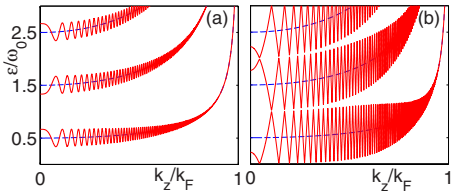

FIG. 9. (Color online) The quasiparticle spectrum for the vortex near the flat surface for (a) $d=2.5\xi$ and (b) $d=1.75\xi$. The CdGM spectrum is shown by the dashed lines. The vortex core profile for a single vortex is approximated by Eq. (40) with $\xi_v = \xi$ and $k_F\xi = 200$.

$$\varepsilon = \omega\left[2n \pm \frac{2k_\perp d + \operatorname{sgn}(h)\tilde{p}^2 \ln(\theta_{\text{th}}\sqrt{|\rho|/\tilde{p}^2})}{\pi}\right]. \tag{85}$$

Here n is an integer, and we have used the asymptotic formula for the argument of gamma function at $\tilde{p} \gg 1$: $\arg[\Gamma(1 - i\tilde{p}^2/2)] \approx -(\tilde{p}^2/2)[\ln(\tilde{p}^2/2) - 1]$. This result coincides with the spectrum obtained from the Bohr-Sommerfeld quantization rule $S(\varepsilon, k_z) = 2\pi n$, where $S(\varepsilon, k_z)$ is given by Eq. (75). The general scenario of spectrum transformation given by Eq. (83) is shown in Fig. 9.

Comparing Figs. 7 and 9 one can see that the spectrum of a vortex approaching the surface is analogous to the spectrum of a two-vortex system where the part of the energy branches [corresponding to the upper or lower sign in Eq. (68)] is omitted. To clarify this result we note that the spectrum transformation in these two situations is brought about by the coupling of trajectories with opposite momentum directions although the origin of coupling is different. It is caused by the normal reflection from the boundary when vortex is situated near the sample surface. For two-vortex or vortex-antivortex systems the coupling occurs due to the intervortex tunneling and the precession of trajectories around the different vortex cores. As we have noticed above in the special case of a vortex near a flat boundary, the spectrum exactly coincides with the spectrum of a vortex-antivortex system if we omit the energy levels corresponding to the even wave functions satisfying $\partial\hat{\Psi}(0, y)/\partial x = 0$.

VII. DENSITY OF STATES

Using the results of the analysis of quasiparticle spectrum transformation under the magnetic-field change, we study the corresponding DOS modification. The calculation of DOS can be done analytically in the quasiclassical limit—i.e., when the energy can be written as a function of the classical impact parameter $b = -\mu/k_\perp$, the trajectory orientation angle θ_p and the momentum projection k_z: $\varepsilon = \varepsilon(\mu/k_\perp, \theta_p, k_z)$. Solving this equation for b, we find a set of isoenergetic curves $\mu_i(\theta_p, \varepsilon, k_z)$. Hereafter we focus on the consideration of DOS contribution coming from a single isoenergetic curve implying that the summation over the index i enumerating different curves should be done.

For each isoenergetic curve the set of energy bands $\varepsilon_n(k_z)$ can be found from the Bohr-Sommerfeld quantization rule,

$$S(\varepsilon_n, k_z) = 2\pi n, \tag{86}$$

where $S(\varepsilon, k_z)$ is the area under the curve $\mu(\theta_p, \varepsilon, k_z)$. The density of states (per unit length and per spin projection) is then given by a standard expression,

$$\nu(\varepsilon) = \sum_n \int_{-k_F}^{+k_F} \frac{dk_z}{2\pi} \delta[\varepsilon - \varepsilon_n(k_z)] = \frac{1}{\pi} \sum_n \left| \frac{\partial \varepsilon_n[k_z = q_n(\varepsilon)]}{\partial k_z} \right|^{-1}, \tag{87}$$

where the energy spectra $\varepsilon_n(k_z)$ are the even functions of momentum due to the symmetry of the BdG equations with respect to the z-axis inversion and $q_n(\varepsilon)$ is a set of positive momenta satisfying the equation $\varepsilon_n(q_n) = \varepsilon$. We also assume here that $|S(\varepsilon, k_z)|$ is a monotonic function of $k_z > 0$ reaching the maximal value at $k_z = 0$. This condition guarantees that we get a single positive q_n root for each energy branch. Such assumption appears to be justified for particular spectrum examples considered above.

Considering the differential of the function $S(\varepsilon, k_z)$ for a fixed n index, we find a simple identity,

$$\frac{\partial \varepsilon_n(k_z)}{\partial k_z} = -\frac{\partial S / \partial k_z}{\partial S / \partial \varepsilon},$$

which allows us to evaluate the derivatives in Eq. (87). As a first step we neglect the discreteness of the energy spectrum and replace the sum over n in Eq. (87) by the corresponding integral. Taking a fixed energy in Eq. (86), one can transform the differential dn as follows:

$$dn = \frac{1}{2\pi} \frac{\partial S}{\partial k_z} dk_z.$$

Finally the expression for DOS reads

$$\nu(\varepsilon) = \frac{1}{4\pi^2} \int_{-k_F}^{k_F} \left| \frac{\partial S}{\partial \varepsilon} \right| dk_z. \tag{88}$$

Taking the spectrum of a singly quantized vortex as an example, we put $\mu = -\varepsilon/\omega$ and obtain, $|S(\varepsilon)| = 2\pi\varepsilon/\omega$ and

$$\nu(\varepsilon) = \nu_0 = \frac{1}{2\pi} \int_{-k_F}^{k_F} \frac{dk_z}{\omega} = \frac{k_F}{4\omega_0}. \tag{89}$$

For a doubly quantized vortex with the spectrum [Eq. (1)] and $\mu_{1,2} = -\varepsilon/\omega \pm \mu^*$, we get $\nu(\varepsilon) = k_F/(2\omega_0) = 2\nu_0$.

Now we proceed with the calculation of DOS for a two-vortex system and for a vortex near the boundary. For the two-vortex system the quasiclassical expression for the area under isoenergetic lines has the form Eq. (49). Therefore, $|\partial S_{1,2}/\partial\varepsilon| = 2\pi/\omega$ and does not depend on the distance between vortices. Thus, the DOS of the two-vortex system is a conserved quantity, which does not depend on the intervortex distance: $\nu(\varepsilon) = k_F/2\omega_0 = 2\nu_0$.

Considering the DOS for a vortex near the boundary of superconductor, we use Eq. (75) and obtain $|\partial S_{1,2}/\partial\varepsilon| = 2\pi/\omega_s$. The important point is that ω_s depends now on the distance from the vortex to the boundary and on the characteristics of the surface (i.e., the focal distance F). The resulting low-energy DOS can be written as follows: $\nu = \nu_0 + \mathrm{sgn}(h)\delta\nu$, where

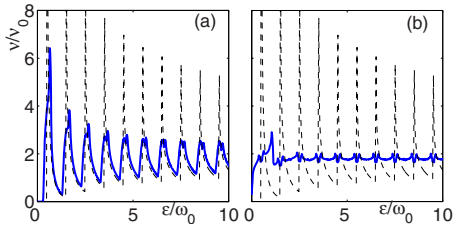

FIG. 10. (Color online) The density of states for a two-vortex system for (a) $a = 5\xi$ and (b) $a = 3.5\xi$. The doubled CdGM DOS is shown by the dashed lines. The vortex core profile for a single vortex is approximated by Eq. (40) with $\xi_v = \xi$ and $k_F\xi = 200$.

$$\delta\nu/\nu_0 = \frac{2\omega_0}{\pi^2 \theta_{\mathrm{th}} k_F d} \int_{-k_F}^{k_F} \frac{\tilde{p}^2}{\omega k_\perp} dk_z, \tag{90}$$

where

$$\tilde{p} = \frac{\Delta_0}{\omega} \frac{e^{-K_0(d)}}{\Lambda \sqrt{k_\perp d} |1 + d/2F|}.$$

The ratio $\delta\nu/\nu_0$ is a monotonically decreasing function of the vortex distance to the surface d and at $d \gg \xi$. It can be evaluated as follows: $\delta\nu/\nu_0 \sim (\xi/d)\exp(-4d/\xi)$. Therefore, if $h < 0$ ($h > 0$), then the DOS is reduced (increased) as the vortex approaches the surface. If the vortex is very close to the surface ($d < |F|$), then h is always negative and therefore the DOS is suppressed. For example, at $d = \xi$ the correction of DOS $\delta\nu$ is of the order of $0.1\nu_0$. This effect can be interpreted as the disappearance of the anomalous spectrum branch occurring as the vortex approaches the boundary and finally leaves the sample. The DOS reduction is the direct consequence of the increase in interlevel distance ω_s [Eq. (76)] in the vortex spectrum due to the appearance of the prohibited domain of trajectory orientation angles as shown in Fig. 8(a). The decrease in the distance d should result in the shrinking of the quasiclassical orbits in (μ, θ_p) space and the DOS suppression until the complete disappearance of the anomalous spectrum branch at the moment of vortex exit.

If the spectrum discreteness cannot be neglected, the above quasiclassical calculation of DOS becomes insufficient. In this case, the rigorous calculation of DOS on the basis of the expression for the quantized spectrum of the two-vortex system [Eq. (68)] and the vortex near the boundary [Eq. (83)] can be done numerically. The results are shown in Figs. 10 and 11. To avoid the singularities, the DOS is averaged over the small energy interval $0.1\omega_0$. In real experimental conditions such smearing of DOS can be caused, e.g., by finite temperature or scattering effects.

The DOS of the two-vortex system (Fig. 10) in the case $a < a_c$ consists of two sets of small peaks shifted by the value $\omega_0(2\chi - [2\chi])$ with background level of $2\nu_0$ [Fig. 10(b)]. Here square brackets denote the integer part and χ is given by Eq. (67). These peaks are van Hove singularities corresponding to the extrema of the spectrum branches at $k_z = 0$ [Fig. 7(b)]. As the distance between vortices increases, the DOS tends to the doubled value of CdGM DOS of the isolated vortex, shown by the dashed lines [Fig. 10(a)].

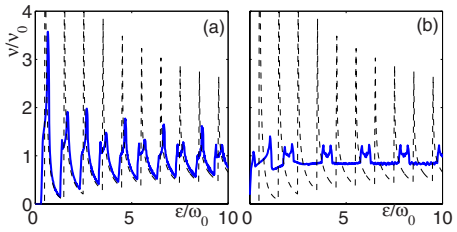

FIG. 11. (Color online) The density of states for a vortex near the flat surface for (a) $d=2.5\xi$ and (b) $d=1.75\xi$. The CdGM DOS is shown by the dashed lines. The vortex core profile for a single vortex is approximated by Eq. (40) with $\xi_v=\xi$ and $k_F\xi=200$.

The expression for the spectrum [Eq. (83)] of a vortex near the boundary is analogous to the spectrum of the two-vortex system where part of the branches corresponding to the upper or lower sign in Eq. (68) is omitted. The function $\nu(\varepsilon)$ for the vortex near the flat boundary is shown in Fig. 11. One can see that similarly to the case of a vortex pair the DOS reveals two sets of peaks, but the energy scale of DOS oscillations is now larger than ω_0.

VIII. HEAT CONDUCTANCE

In this section we calculate the heat conductance of vortex states in a mesoscopic superconductor focusing on the low-temperature limit $T \ll \Delta_0$ when the transport is dominated by the contribution of subgap levels. We consider the ballistic regime and neglect the scattering effects on the boundaries between superconductor and normal-metal leads. The expression for the thermal conductance reads[14]

$$\kappa = \frac{1}{4\pi\hbar T^2}\sum_n \int_0^{k_F} \frac{\varepsilon_n^2}{\cosh^2(\varepsilon_n/2T)}\left|\frac{\partial \varepsilon_n}{\partial k_z}\right| dk_z. \tag{91}$$

Let us introduce the function $N(\varepsilon)$ giving the number of energy branches crossing a certain energy level ε;

$$N(\varepsilon) = \sum_n \int_0^{k_F} dk_z \delta[\varepsilon - \varepsilon_n(k_z)]\left|\frac{\partial \varepsilon_n}{\partial k_z}\right|. \tag{92}$$

Then the expression (91) can be rewritten as follows:

$$\kappa = \frac{1}{4\pi\hbar T^2}\int_0^{\infty} \frac{\varepsilon^2 N(\varepsilon)}{\cosh^2(\varepsilon/2T)} d\varepsilon. \tag{93}$$

In the temperature interval $\omega_0 \lesssim T \ll \Delta_0$ the discreteness of the spectrum can be neglected. In order to evaluate the number of states $N(\varepsilon)$ in Eq. (93), we use the quasiclassical theory assuming that the probability of Landau-Zener tunneling between different quasiclassical orbits is small. Generally, the quasiclassical theory is valid only within the momentum interval $k_z < k_z^*$, otherwise the interband Landau-Zener transitions cannot be neglected. As a result, in Eq. (92) we should take the upper limit of integration k_z^* instead of k_F. The value of the threshold momentum $k_\perp^*$ can be estimated from the condition that the Landau-Zener tunneling probability W [see Eq. (7)] is equal to a certain threshold value $W_{\rm th} < 1$. Using the Bohr-Sommerfeld quantization rule [Eq. (86)], we find:

$$N(\varepsilon) = \left|\int_0^{k_z^*} \frac{dS(\varepsilon,k_z)}{dk_z}\frac{dk_z}{2\pi}\right| = \frac{|S(\varepsilon,0) - S(\varepsilon,k_z^*)|}{2\pi}. \tag{94}$$

To evaluate the integral [Eq. (93)], we consider the Taylor expansion $|S(\varepsilon,0) - S(\varepsilon,k_z^*)| = \Sigma_{n=0}^{\infty} S^{(n)}\varepsilon^n/n!$, where

$$S^{(n)} = \left.\frac{d^n}{d\varepsilon^n}|S(\varepsilon,0) - S(\varepsilon,k_z^*)|\right|_{\varepsilon=0}.$$

As a result, we find the expansion of the heat conductance in power series of T,

$$\kappa = \frac{T}{4\pi\hbar}\sum_{n=0}^{\infty} A_n S^{(n)} T^n, \tag{95}$$

where A_n are expressed in terms of the Rihmann function $\zeta(n)$:

$$A_n = \frac{2(n+2)(n+1)}{\pi}[1 - 2^{-(n+1)}]\zeta(n+2).$$

Consequently the effective number of conducting modes $N_v = \kappa/\kappa_0$ is

$$N_v = \frac{3}{4\pi^2}\sum_{n=0}^{\infty} A_n S^{(n)} T^n. \tag{96}$$

For a singly quantized vortex we get $N(\varepsilon) = \varepsilon/\omega_0$ and

$$N_v = \frac{27\zeta(3)}{2\pi^2}\frac{T}{\omega_0},$$

which coincides with the expression obtained in Ref. 14. For a doubly quantized vortex $N(\varepsilon) = 2\mu^*$, where $\mu^* \sim k_F\xi$ and $N_v = \mu^*$. Now we proceed with the calculation of the heat conductance for the two-vortex system and for the vortex near the sample surface.

A. Two-vortex system

The results of our numerical calculation of the number of conducting modes as a function of temperature on the basis of Eq. (91) with the spectrum Eq. (68) are shown in Fig. 12. The suppression of N_v at $T \ll \omega_0$ is caused by the minigap in the spectrum. One can see that at $T \gtrsim \omega_0$ the function $N_v(T)$ grows linearly with T. Extrapolating this linear dependence to $T=0$, we find the residual number of modes N_0—which is plotted by the solid curve in Fig. 13 as a function of the intervortex distance a.

The quasiclassical procedure suggested in the beginning of this section allows us to obtain a good analytical approximation describing the behavior of the residual number of modes for $a < a_c$. To get such approximation, we evaluate the temperature-independent term $N_0 = N(0)/2$ in expansion (96), which dominates for rather small intervortex distances $a < a_c$. We use expression (94) for the number of states $N(\varepsilon)$ where the area confined by the closed orbits in (μ, θ_p) space is given by Eq. (47). The resulting number of conducting modes vs intervortex distance is shown in Fig. 13 by the dashed curve. Here we choose the threshold probability $W_{\rm th} = 0.54$ to obtain a reasonable fit to the numerical results

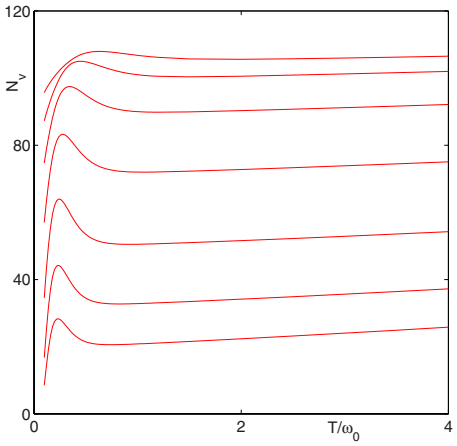

FIG. 12. (Color online) Temperature dependence of the number of conducting modes N_v for a two-vortex system. Curves are plotted for $a=2\xi$ to $a=5\xi$ with the step 0.5ξ (from top to bottom). The vortex core profile for a single vortex is approximated by Eq. (40) with $\xi_v=\xi$ and $k_F\xi=200$.

(solid curve) at $a\sim 2\xi$. The critical distance a_c is defined by $N_0(a_c)=0$. The chosen value of the threshold probability corresponds to the critical intervortex distance $a_c\simeq 4.5\xi$.

For well separated vortices, i.e., when $a>2\xi$, the splitting of energy branches is small. One can use approximate expression (71) for the area $S(\varepsilon,k_z)$ to obtain

$$N_0=\frac{a}{\pi}(k_F-k_\perp^*)+\frac{p^2}{\pi}\ln(\theta_{\rm th}\sqrt{k_F a/p^2}), \tag{97}$$

where

$$k_\perp^*=k_F\frac{\sqrt{(a/\xi_v)^2+4}-2}{\sqrt{(a_c/\xi_v)^2+4}-2}. \tag{98}$$

This expression coincides with the estimate [Eq. (10)] in the limit $a\gg\xi_v$.

B. Vortex near the sample boundary

The calculation of the number of conducting modes for the vortex near the boundary can be carried out similarly to the above analysis of the two-vortex system. We restrict ourselves to the case when the vortex is situated not very close to the boundary: $d\gtrsim\xi$, when we can neglect the distortion of vortex core profile due to boundary effects. Taking for example a flat surface ($h=-1$ and $F=\infty$), we use Eqs. (83) and (91) and calculate the residual number of conducting modes N_0 obtained from the extrapolation of the linear parts of $N_v(T)$ dependencies to $T=0$. In Fig. 14 we plot the resulting dependence $N_0(d)$ (solid curve).

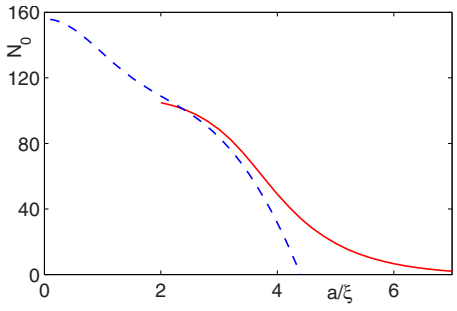

FIG. 13. (Color online) Residual number of modes as a function of the intervortex distance. Solid line shows the result of the exact calculation based on Eq. (91), while dashed line is obtained from the analytical approximate expressions (47) and (96).

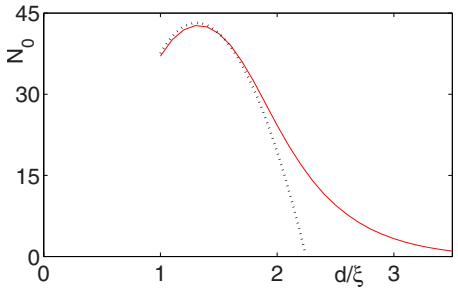

FIG. 14. (Color online) Residual number of modes N_0 as a function of the distance to the surface d. Solid line shows the result of the exact calculation based on Eq. (91), while dashed line is obtained from the analytical formula (99). The vortex core profile for a single vortex is approximated by Eq. (40) with $\xi_v=\xi$ and $k_F\xi=200$.

The estimate of the residual number of conducting modes within the quasiclassical theory yields the following result:

$$N_0=\frac{d}{\pi}(k_F-k_\perp^*)+\mathrm{sgn}(\kappa)\frac{\tilde{p}^2}{2\pi}\ln(\theta_{\rm th}\sqrt{|\rho|/\tilde{p}^2}), \tag{99}$$

where

$$k_\perp^*=k_F\frac{\sqrt{(d/\xi_v)^2+1}-1}{\sqrt{(d_c/\xi_v)^2+1}-1}, \tag{100}$$

for the particular vortex core model Eq. (40). Taking $d_c\simeq 2.25\xi$, we plot approximate expression (99) for $N_0(d)$ in Fig. 14 (dashed curve).

One can see that the normal reflection at the surface leads to the essential increase in the residual number of conducting modes with the decrease in the distance d. This effect is a consequence of the minigap suppression. The nonmonotonic behavior of $N_0(d)$ at the distances $d\sim\xi$ has the same origin as the decrease in the zero energy DOS, which occurs at these distances. The residual number of conducting modes $N_0(d)$ is defined by the number of states at the zero energy level $N(0)$ [see Eq. (95)], which is proportional to the area enclosed by the quasiclassical orbits in (μ,θ_p) space. Therefore the shrinking of closed quasiclassical orbits at $d\sim\xi$ results in the decrease in the $N_0(d)$ value. At small distances to the surface $d<\xi_v$ our approach does not work. However it is natural to expect further suppression of the number of subgap conducting modes down to zero, which accompanies the vortex exit from the sample.

C. Magnetic-field dependence of thermal conductance

To illustrate our analysis of the heat transport in the vortex state, it is useful to consider the magnetic-field depen-

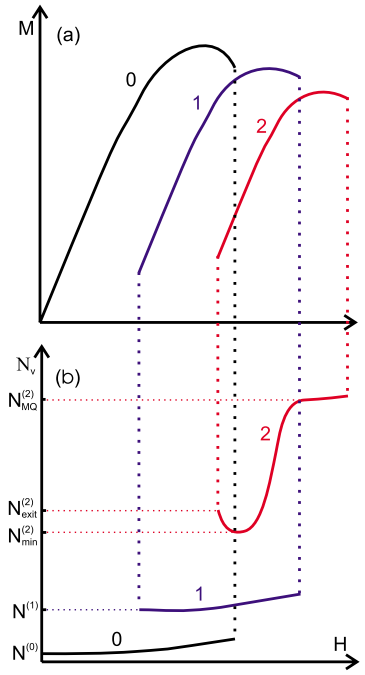

FIG. 15. (Color online) (a) Schematic plots of magnetization and (b) effective number of modes contributing to the heat conductance in a mesoscopic sample vs applied magnetic field. Different branches correspond to the states with different number of vortices trapped in the sample.

dence of the heat conductance caused by the transformation of the vortex structure. For this purpose we plot the schematic dependencies of the sample magnetization and the effective number of modes at a certain finite temperature $T \gtrsim \omega_0$ as shown in Fig. 15. Different branches of the magnetization curve shown in Fig. 15(a) correspond to the different number of vortices in the superconducting sample. Starting from small magnetic fields $H \ll H_{c2}$, the sample is in the Meissner state—i.e., the number of vortices is zero. The number of conducting modes $N_v = \kappa/\kappa_0$ [see Fig. 15(b)] is determined by quasiparticle states with energies above the superconducting gap Δ_0 and therefore is exponentially small $N_v = N^{(0)} \sim (k_F L)^2 e^{-\Delta_0/T}$ provided $T \ll T_c$, where L is a characteristic transverse size of the sample. In increasing magnetic field the superconducting gap is suppressed leading to a slightly growing N_v. When the magnetic field becomes large enough to introduce a vortex into the sample, the number of conducting modes jumps to the value $N^{(1)} \sim T/\omega_0$ simultaneously with the vortex entry. This increase in N_v is caused by the appearance of subgap quasiparticle states localized within the vortex core.[14] The next jump in the number of conducting modes occurs together with the second vortex entry. If the sample geometry favors the formation of a giant doubly quantized vortex, the number of conducting modes rises up to the value $N^{(2)}_{MQ} \sim (k_F \xi)$. At the interval of magnetic fields where the giant vortex is stable, N_v is almost constant. The decay of the giant vortex into singly quantized vortices in decreasing magnetic field is accompanied by the decrease in N_v up to the value $N^{(2)}_{\min} \gtrsim 2N^{(1)}$ (see Sec. V for details). While the distance between the vortices grows, they approach the sample surface and the number of conducting modes increases again (as it was shown in Sec. IV). This increase is cut off at a certain value $N^{(2)}_{\text{exit}}$ at the field corresponding to the vortex exit.

IX. SUMMARY

To summarize, we suggest a description of a subgap quasiparticle spectrum in the multivortex state of a mesoscopic superconductor. Considering multiquantum (giant) vortices, we have obtained a general analytical expression for the quasiparticle spectrum—which is valid for any value of vorticity and arbitrary vortex core model. Taking the simplest example of the doubly quantized vortex, we have considered the evolution of the anomalous spectrum branches—which accompanies the splitting of the doubly quantized vortex. Considering the limit of well separated vortices, we have found the spectrum of vortex clusters bonded by the quasiparticle tunneling and have investigated the crossover to the Caroli–de Gennes–Matricon spectrum of isolated vortices. We have shown that the minigap in the quasiparticle spectrum is absent for the intervortex distances $a < a_c \approx \xi \ln(k_F \xi)$. In mesoscopic superconductors it is necessary also to take account of the normal reflection of quasiparticles at the sample surface. We have shown that the spectrum of a single vortex placed near the parabolic surface is transformed analogously to the two-vortex system and the minigap in the spectrum is suppressed when the distance from the vortex to the surface is less than the critical value: $d < d_c \approx (\xi/2)\ln(k_F \xi)$. When the distance is of the order of the vortex core size, the interlevel spacing in the vortex spectrum becomes larger than the CdGM value. This effect leads to the disappearance of the anomalous spectrum branch when the vortex approaches the surface.

We have analyzed the quasiparticle density of states and the heat conductance along the magnetic field, which are determined by the anomalous branches of the quasiparticle spectrum. At the temperatures $T \gg \omega_0$ neglecting the discreteness of spectrum we have obtained a general expression for the DOS and heat conductance through the characteristics of the quasiclassical orbits in (μ, θ_p) space. Applying the general formula to the vortex pair, we have observed a significant decrease in the heat conductance as a function of the growing intervortex distance. Even in the limit of the zero intervortex distance—i.e., for a doubly quantized vortex—the number of conducting modes $N_v \sim k_F \xi$ appears to be much less than the value $(k_F \xi)^2$, which determines the number of conducting modes for a normal-metal wire of the radius ξ. At nonzero intervortex distances and in the temperature region $\omega_0 < T \ll \Delta_0$ the effective number of transport modes is a linear function of temperature; $N_v = N_0 + \alpha T$. The splitting of the doubly quantized vortex is accompanied by the decrease in the residual number of modes N_0, and at rather large intervortex distances we get the doubled heat conductance of a single vortex; $N_v \sim T/\omega_0 \ll k_F \xi$.

Also we have shown that the normal reflection at the surface of the sample leads to a considerable increase in the heat conductance along the magnetic field when the distance from the vortex to the sample boundary becomes rather small: $\xi \lesssim d < d_c$. The exit of a vortex from the sample is accompa-

nied by the disappearance of the anomalous spectrum branch and, therefore, both the heat conductance and the DOS are suppressed at $d \lesssim \xi$.

ACKNOWLEDGMENTS

We thank N. B. Kopnin and G. E. Volovik for the stimulating discussions, I. A. Shereshevskii and V. I. Pozdnyakova for the help with computer codes, and S. V. Sharov for the valuable comments. This work was supported, in part, by Russian Foundation for Basic Research, by Program "Quantum Macrophysics" of RAS, and by Russian Science Support and "Dynasty" Foundations.

APPENDIX A: DERIVATION OF EQ. (59)

At first let us prove the following formula:

$$\int_{-\infty}^{\infty} e^{-ik^2/2+ikx} F(k)dk = \sqrt{2\pi i}\int_{-\infty}^{\infty} e^{i(x-y)^2/2} f(y)dy, \quad \text{(A1)}$$

where $f(x)$ is a smooth enough function defined at $-\infty < x < \infty$ and $F(k)=2\pi\int_{-\infty}^{\infty} e^{-ikx} f(x)dx$. Indeed, the integral in the right-hand side of Eq. (A1) can be written as follows:

$$\int_{-\infty}^{\infty} e^{i(x-y)^2/2} f(y)dy = \int\int_{-\infty}^{\infty} e^{i(x-y)^2/2+iky} F(k)dkdy.$$

Noting that $(x-y)^2/2+ky=(y+k-x)^2/2+kx-k^2/2$, we integrate over the y variable using the formula $\int_{-\infty}^{\infty} e^{ix^2}dx=\sqrt{\pi i}$ and obtain

$$\int\int_{-\infty}^{\infty} e^{i(x-y)^2/2+iky} F(k)dkdy = \frac{1}{\sqrt{2\pi i}}\int_{-\infty}^{\infty} e^{-ik^2/2+ikx} F(k)dk.$$

Taking Eq. (58) in the form,

$$\left[\int_{\infty}^{\infty} e^{i\mu^2/k_\perp a}(e^{-K_0(a/2)} - i\hat{\gamma}\hat{\sigma}_z)\hat{\lambda} e^{i\mu\theta_1} c_\mu d\mu\right] = e^{-2i\varphi}\left[\int_{\infty}^{\infty} e^{-i\mu^2/k_\perp a}(e^{-K_0(a/2)} + i\hat{\gamma}\hat{\sigma}_z)\hat{\lambda}^* e^{-i\mu\theta_1} c_\mu^* d\mu\right], \quad \text{(A2)}$$

we multiply it by $e^{ik_\perp a(\theta-\theta_1)^2/4}$ and integrate over θ_1. Using Eq. (A1) we can transform the above integrals as follows:

$$\int\int_{-\infty}^{\infty} e^{ik_\perp a(\theta-\theta_1)^2/4} e^{i\mu^2/k_\perp a} e^{i\mu\theta_1} c_\mu d\mu d\theta_1 = \sqrt{\frac{2\pi}{i}}\int\int_{-\infty}^{\infty} e^{i(k_\perp a/4)[(\theta-\theta_1)^2-(\theta_1-\theta_2)^2]} C(\theta_2)d\theta_1 d\theta_2 = \frac{\sqrt{2/i\pi}}{k_\perp a} C(\theta),$$

$$\int\int_{-\infty}^{\infty} e^{ik_\perp a[(\theta-\theta_1)^2/4-\theta^2/2]} e^{-i\mu^2/k_\perp a} e^{-i\mu\theta_1} c_\mu^* d\mu = \sqrt{2\pi i}\int\int_{-\infty}^{\infty} e^{ik_\perp a[(\theta-\theta_1)^2/4+(\theta_1-\theta_2)^2/4-\theta_1^2/2]} C(\theta_2)d\theta_1 d\theta_2 = \frac{\sqrt{2i/\pi}}{k_\perp a} e^{ik_\perp a\theta^2/2} C^*(-\theta).$$

Making use of these expressions, the derivation of Eq. (59) from Eq. (A2) is straightforward.

APPENDIX B: TRANSFER MATRICES

Let us consider the following system of equations:

$$i\frac{\partial}{\partial x}B_1 + xB_1 = pB_2,$$

$$i\frac{\partial}{\partial x}B_2 - xB_2 = pB_1, \quad \text{(B1)}$$

where $p>0$ and x is a coordinate along real or imaginary axes. We start with the case of real x. Solutions of Eqs. (B1) can be expressed in terms of the parabolic cylinder functions D (Ref. 19) with arbitrary constants d_1 and d_2:

$$B_1 = d_1 D_{ip^2/2}\left(x\sqrt{\frac{2}{i}}\right) + d_2 D_{ip^2/2}\left(-x\sqrt{\frac{2}{i}}\right),$$

$$B_2 = \frac{p}{\sqrt{2i}}\left[d_1 D_{ip^2/2-1}\left(x\sqrt{\frac{2}{i}}\right) - d_2 D_{ip^2/2-1}\left(-x\sqrt{\frac{2}{i}}\right)\right]. \quad \text{(B2)}$$

The asymptotic expressions for the obtained solutions for $x \gg \max(1,p)$ are the following:

$$D_{ip^2/2}\left(x\sqrt{\frac{2}{i}}\right) \simeq e^{ix^2/2+i(p^2/2)\ln(\sqrt{2}x)+\pi p^2/8},$$

$$D_{ip^2/2-1}\left(x\sqrt{\frac{2}{i}}\right) \simeq 0,$$

$$D_{ip^2/2}\left(-x\sqrt{\frac{2}{i}}\right) \simeq e^{ix^2/2+i(p^2/2)\ln(\sqrt{2}x)-3\pi p^2/8},$$

$$D_{ip^2/2-1}\left(-x\sqrt{\frac{2}{i}}\right) \simeq \sqrt{2\pi}\frac{e^{-ix^2/2-i(p^2/2)\ln(\sqrt{2}x)-\pi p^2/8}}{\Gamma(1-ip^2/2)},$$

where Γ is the gamma function. Then, we find the scattering matrix $\hat{X}_1$ coupling the solutions $\hat{B}=(B_1,B_2)$ at $x>0$ and $x<0$;

$$\hat{B}(x>0) = \hat{X}_1\hat{B}(x<0),$$

in the following form:

$$\hat{X}_1 = e^{-\pi p^2/2}\hat{I} + i(\hat{\sigma}_y \,\mathrm{Re}\,\tau_1 + \hat{\sigma}_x \,\mathrm{Im}\,\tau_1), \quad \text{(B3)}$$

where $\hat{I}$ is the unity matrix,

$$\tau_1 = \sqrt{2\ \sinh(\pi p^2/2)}e^{-\pi p^2/4}e^{i\chi_1},$$

and $\chi_1 = x^2 + p^2\ \ln|\sqrt{2}x| + \arg\ \Gamma(1-p^2/2) + \pi/4$.

Next, we consider the case of imaginary coordinate x. Introducing a new variable $y=-ix$, we obtain an analytical continuation of the solutions [Eq. (B2)]:

$$B_1 = d_1 D_{ip^2/2}(y\sqrt{2i}) + d_2 D_{ip^2/2}(-y\sqrt{2i}),$$

$$B_2 = \frac{p}{\sqrt{2i}}[d_1 D_{ip^2/2-1}(y\sqrt{2i}) - d_2 D_{ip^2/2-1}(-y\sqrt{2i})].$$

The asymptotic expressions for this solutions at $y \gg \max(1,p)$ have the form:

$$D_{ip^2/2}(y\sqrt{2i}) \simeq e^{-iy^2/2+i(p^2/2)\ln(\sqrt{2}y)-\pi p^2/8},$$

$$D_{ip^2/2-1}(y\sqrt{2i}) \simeq 0,$$

$$D_{ip^2/2}(-y\sqrt{2i}) \simeq e^{-iy^2/2+i(p^2/2)\ln(\sqrt{2}y)+3\pi p^2/8},$$

$$D_{ip^2/2-1}(-y\sqrt{2i}) \simeq \sqrt{2\pi}\frac{e^{iy^2/2-i(p^2/2)\ln(\sqrt{2}y)+\pi p^2/8}}{\Gamma(1-ip^2/2)},$$

and the transfer matrix is

$$\hat{X}_2 = e^{\pi p^2/2}\hat{I} + (\hat{\sigma}_y\ \mathrm{Re}\ \tau_2 + \hat{\sigma}_x\ \mathrm{Im}\ \tau_2), \tag{B4}$$

where

$$\tau_2 = \sqrt{2\ \sinh(\pi p^2/2)}e^{\pi p^2/4}e^{i\chi_2},$$

and

$$\chi_2 = y^2 - p^2\ \ln|\sqrt{2}y| - \arg\ \Gamma(1-p^2/2) + \pi/4.$$

[1] G. Boato, G. Gallinaro, and C. Rizutto, Solid State Commun. **3**, 173 (1965); D. S. McLachlan, *ibid.* **8**, 1589 (1970); L. F. Chibotaru, A. Ceulemans, V. Bruyndoncx, and V. V. Moshchalkov, Nature (London) **408**, 833 (2000).

[2] V. A. Schweigert, F. M. Peeters, and P. S. Deo, Phys. Rev. Lett. **81**, 2783 (1998).

[3] A. K. Geim, S. V. Dubonos, J. J. Palacios, I. V. Grigorieva, M. Henini, and J. J. Schermer, Phys. Rev. Lett. **85**, 1528 (2000).

[4] V. V. Shmidt and G. S. Mkrtchyan, Usp. Fiz. Nauk **112**, 459 (1974) [Sov. Phys. Usp. **17**, 170 (1974)]; G. R. Berdiyorov, B. J. Baelus, M. V. Milošević, and F. M. Peeters, Phys. Rev. B **68**, 174521 (2003).

[5] A. Kanda, B. J. Baelus, F. M. Peeters, K. Kadowaki, and Y. Ootuka, Phys. Rev. Lett. **93**, 257002 (2004); B. J. Baelus, A. Kanda, F. M. Peeters, Y. Ootuka, and K. Kadowaki, Phys. Rev. B **71**, 140502(R) (2005); B. J. Baelus, A. Kanda, N. Shimizu, K. Tadano, Y. Ootuka, K. Kadowaki, and F. M. Peeters, *ibid.* **73**, 024514 (2006).

[6] C. Caroli, P. G. de Gennes, and J. Matricon, Phys. Lett. **9**, 307 (1964).

[7] A. S. Mel'nikov and M. A. Silaev, Pis'ma Zh. Eksp. Teor. Fiz. **83**, 675 (2006) [JETP Lett. **83**, 578 (2006)].

[8] G. E. Volovik, Pis'ma Zh. Eksp. Teor. Fiz. **57**, 233 (1993) [JETP Lett. **57**, 244 (1993)].

[9] Y. Tanaka, A. Hasegawa, and H. Takayanagi, Solid State Commun. **85**, 321 (1993); Y. Tanaka, S. Kashiwaya, and H. Takayanagi, Jpn. J. Appl. Phys., Part 1 **34**, 4566 (1995); D. Rainer, J. A. Sauls, and D. Waxman, Phys. Rev. B **54**, 10094 (1996); S. M. M. Virtanen and M. M. Salomaa, *ibid.* **60**, 14581 (1999); M. Eschrig, D. Rainer, and J. A. Sauls, in *Vortices in Unconventional Superconductors and Superfluids*, edited by R. P. Huebener, N. Schopohl, and G. E. Volovik (Springer-Verlag, Berlin, 2001); K. Tanaka, I. Robel, and B. Janko, Proc. Natl. Acad. Sci. U.S.A. **99**, 5233 (2002).

[10] A. S. Mel'nikov and V. M. Vinokur, Nature (London) **415**, 60 (2002); Phys. Rev. B **65**, 224514 (2002).

[11] A. I. Larkin and Yu. N. Ovchinnikov, Phys. Rev. B **57**, 5457 (1998).

[12] S. Graser, C. Iniotakis, T. Dahm, and N. Schopohl, Phys. Rev. Lett. **93**, 247001 (2004).

[13] N. B. Kopnin, A. S. Mel'nikov, V. I. Pozdnyakova, D. A. Ryzhov, I. A. Shereshevskii, and V. M. Vinokur, Phys. Rev. Lett. **95**, 197002 (2005).

[14] N. B. Kopnin, A. S. Mel'nikov, V. I. Pozdnyakova, D. A. Ryzhov, I. A. Shereshevskii, and V. M. Vinokur, Phys. Rev. B **75**, 024514 (2007).

[15] N. B. Kopnin, A. S. Mel'nikov, and V. M. Vinokur, Phys. Rev. B **68**, 054528 (2003).

[16] L. D. Landau and E. M. Lifshitz, *Quantum Mechanics: Non-Relativistic Theory* (Pergamon, New York, 1991).

[17] N. B. Kopnin and G. E. Volovik, Pis'ma Zh. Eksp. Teor. Fiz. **64**, 641 (1996) [JETP Lett. **64**, 690 (1996)]; N. B. Kopnin, Phys. Rev. B **57**, 11775 (1998).

[18] E. O. Kane and E. I. Blount, in *Tunneling Phenomena in Solids*, edited by E. Burstein and S. Lundqvist (Plenum, New York, 1969).

[19] E. T. Whittaker and G. N. Watson, *Modern Analysis* (Cambridge University Press, Cambridge, 1947), Chap. 16.